Analysis of Stroke on Brain Computed Tomography Scans

Thesis submitted in partial fulfillment
of the requirements for the degree of

M.S.
in
Computer Science

by

Saurabh Sharma
200502024
saurabhsharma@research.iiit.ac.in

Center for Visual Information Technology
International Institute of Information Technology
Hyderabad - 500 032, INDIA
October 2013

International Institute of Information Technology
Hyderabad, India

CERTIFICATE

It is certified that the work contained in this thesis, titled "Analysis of Stroke on Brain Computed Tomography Scans" by Saurabh Sharma, has been carried out under my supervision and is not submitted elsewhere for a degree.

______________	___________________________________
Date	Adviser: Prof. Jayanthi Sivaswamy

To MY PARENTS

Abstract

Stroke is one of the leading causes of death and disability in the world. Early detection of Stroke (both hemorrhagic and ischemic) is very important as it can ensure up to full recovery. Timely detection of stroke, especially ischemic stroke is difficult as the changes in abnormal tissue only become visible after the damage has already been done. The detection is even more difficult on CT scan compared to other imaging modalities but the dependence of a large fraction of population on CT, makes the need to find a solution to the problem even more imperative. Though the detection accuracy of radiologists for early stroke depends on various factors like experience, available technology, etc., earlier estimates put the accuracy around 10% [45]. Even with considerable advancement in CT technology the performance has still only increased to around 70% or thereabouts [21]. Any kind of assistance to radiologists which can improve their detection accuracy would therefore be much appreciated. This thesis presents a framework for automatic detection and classification of different types of stroke. We characterize stroke as a distortion in the otherwise contralaterally similar distribution of brain tissue. Classification depends on the severity of the distortion with hemorrhage and chronic infarcts exhibiting the maximum distortion and hyperacute stroke showing the minimum. The detection work on hemorrhagic stroke and early ischemic stroke has clinical value whereas the work on later stages of ischemic stroke has mainly academic use. The automatic detection approach was tested on a dataset containing 19 normal (291 slices) and 23 abnormal (181 slices) datasets. The algorithm gave a high recall rate for hemorrhage (80%), chronic (95%), acute (91.80%) and hyperacute (82.22%) stroke at slice level. The corresponding precision figures were 93.3%, 90.47%, 87.5% and 69.81% respectively. The performance of the system in a normal vs. stroke-affected scenario was 83.95% precision and 86.74% recall. The lower precision value in case of hyperacute scans is because of large number of normal slices with slight disturbances in contra-lateral symmetry being identified as stroke cases. We also present a novel approach for enhancement of early ischemic stroke regions using image-adaptive window parameters, to aid the radiologists in the manual detection of early ischemic stroke. The enhancement approach increased the average accuracy of radiologists in clinical conditions from around 71% to around 90% (p=0.02, two tailed student's t test) with the inexperienced radiologists benefitting more from the enhancement. The average reviewing time of the scans was also reduced from about 9 to 6 seconds per slice. Out of the two approaches, automatic detection and enhancement, results show the enhancement process to be more promising.

Contents

Chapter Page

1 Introduction . . . 1
1.1 Medical Background . . . 2
1.1.1 Human Brain . . . 2
1.1.2 Brain Stroke . . . 2
1.1.3 Imaging the Brain . . . 3
1.1.4 Stroke in Brain CT . . . 5
1.2 Why Unenhanced CT . . . 7
1.3 Earliest Visible Signs of Acute Infarct . . . 7
1.4 Problem Statement and Contribution . . . 9
1.4.1 Track 1 . . . 9
1.4.2 Track 2 . . . 10
1.5 Thesis Structure . . . 10

2 Related Work . . . 12
2.1 Hemorrhage Detection . . . 12
2.2 Ischemic Stroke . . . 13
2.3 Ischemic Stroke Enhancement . . . 14

3 Automatic Stroke Detection . . . 16
3.1 Preprocessing . . . 16
3.2 Mid-Sagittal Plane Detection and Rotation Correction . . . 17
3.3 Stroke Detection and Identification . . . 19
3.3.1 Level 1 Classification . . . 19
3.3.2 Level 2 Classification . . . 19
3.3.3 Level 3 Classification . . . 20
3.3.3.1 Contrast Enhancement . . . 23
3.3.3.2 Tissue Segmentation . . . 24
3.3.3.3 Candidate Selection . . . 25
3.3.3.4 Hyperacute Infarct Region Detection . . . 26
3.4 Results and Discussion . . . 26
3.4.1 Dataset Details . . . 26
3.4.2 Detection Results and Discussion . . . 27

4 Enhancement of Early Infarct through Auto-Windowing 32
4.1 Manual Windowing 32
4.2 Region Based Windowing 36
4.3 Pixel Based Windowing 36
4.3.0.1 Parzen Window 37
4.3.0.2 Parzen Based Windowing 38
4.4 Results 39
4.4.1 Experiment Details 39
4.4.2 Discussion 40

5 Conclusions 42
5.1 Automatic Detection 42
5.2 Enhancement of Affected Tissue 43

Bibliography 46

List of Figures

Figure Page

1.1 Axial view of gray and white matter [38] . . . 2
1.2 Representation of various types of stroke and normal brain . . . 3
1.3 Representation of brain under various modalities . . . 3
1.4 Tissue definition on CT . . . 4
1.5 A volume CT scan of a normal brain . . . 6
1.6 Appearance of early infarct on CT and MR . . . 7
1.7 Various signs of early infarct [5], [40] . . . 8
1.8 Automatic stroke detection framework . . . 9

3.1 Preprocessing results . . . 17
3.2 Nose extraction . . . 18
3.3 Rotation correction results . . . 18
3.4 Histograms obtained at level 1 . . . 19
3.5 Histograms acute infarct . . . 20
3.6 Rough segmentation of gray white matter on CT . . . 21
3.7 Algorithm outline . . . 24
3.8 Extraction of hypodense pixels. . . . 25
3.9 Images from samples of different stroke cases . . . 28
3.10 Images from samples of different stroke cases . . . 29
3.11 Comparison of missed hyperacute boundary slice with normal slice . . . 30
3.12 Hyperacute failure case (infarct indicated by arrow) . . . 31

4.1 Demonstration of windowing process . . . 33
4.2 Representation of contrast stretching/ compressing (windowing) . . . 34
4.3 Stroke appearance under reduced window settings (center, width). . . . 35
4.4 Histograms of V_i and V_{ic} . . . 36
4.5 Images from samples of different stroke cases . . . 37
4.6 Parzen-based windowing results . . . 40

5.1 Appearance of early tumor lesions on CT scan [43] . . . 44

List of Tables

Table		Page
1.1	Hounsfield scale	5
3.1	CT acquisition protocol	26
3.2	Results of the complete system at slice level	27
3.3	Results depicting clinical scenario	29
3.4	Patient level results of the complete system	30
3.5	Table showing system level performance	31
4.1	Clinical study results	40

Chapter 1

Introduction

Stroke (formerly cerebrovascular accident, CVA) is a leading cause of death and disability in the world. According to the World Health Organization, 15 million people suffer from stroke, of these 5 million die and another 5 million are permanently disabled. The emergence of various medical imaging technologies like Computed Tomography (CT), Magnetic Resonance Imaging (MRI), Positron Emission Tomography (PET), etc., have contributed positively towards visualization and diagnosis of various complications of brain. These modalities have also been largely responsible for opening new avenues of research for improving the efficiency of radiologists through automated analysis.

Stroke is characterized by a disturbance in blood flow to the brain resulting either in ischemic or hemorrhagic stroke. Hemorrhage occurs due to bursting of blood vessel in the brain whereas ischemic stroke is the result of a blockage in the blood vessel which inhibits the blood supply to brain. Though both being fatal in nature, complete recovery can be achieved in fair number of patients suffering from hemorrhage whereas the chances of complete recovery are considerably less in case of ischemic stroke. In fact, the recovery from ischemic stroke depends on the timing of treatment which can only be performed within the first few hours [0-4 hrs.] from the onset. The golden rule of ischemic stroke is ”Time is Brain” since with the passage of each second of time, more and more brain tissues suffer irreversible damage. When compared to normal brain aging, each hour of untreated stroke ages a brain by about 3.6 years [36]. This makes the early detection of both hemorrhagic and ischemic stroke of utmost clinical importance.

The rest of the chapter will shed further light on the nature of brain, stroke and the various modalities used to image the brain. This will be followed by the summary of thesis contribution and the structure of the rest of the thesis.

1.1 Medical Background

1.1.1 Human Brain

The human brain is the center of the central nervous system and is responsible for regulating the body's actions and reactions. The brain is enclosed in a thick skull and suspended in a clear bodily liquid called cerebrospinal fluid (CSF) which acts as a buffer for the brain in case of sudden jolts. CSF is mostly made up of white blood cells, enzymes and glucose. The brain can be described as being consisting of two major types of tissues, the gray matter and white matter. The gray matter tissues consist of neuronal cells, glial cells and capillaries and perform most of the brain functions. The white matter mainly consists of bundles of myelinated axons and connects the various gray matter areas of the brain. Figure. 1.1 shows the distribution of gray and white matter tissues in an axial cerebrum slice.

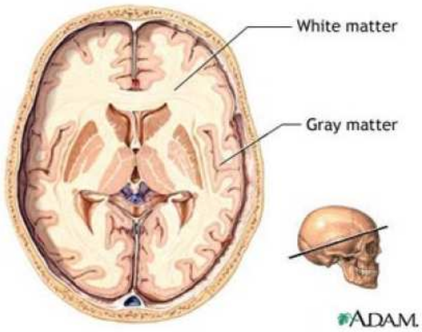

Figure 1.1 Axial view of gray and white matter [38]

1.1.2 Brain Stroke

Being the control center of the human body, brain requires a large chunk of body resources in order to carry out its vital functions. Around 20 % oxygen and blood supply is used by the brain alone and any disturbance in supply of these resources can lead to complications, which in many cases can prove fatal. Stroke is one such complication which can occur in the form of ischemic and hemorrhagic stroke. Around 80% stroke are ischemic in nature. Ischemic stroke are further divided into *hyperacute, acute and chronic* infarction based on the time passed since the onset of symptoms with hyperacute being the earliest stage and chronic being the latter stage at which point most of time most of the tissues have undergone irreparable damage. Figure. 1.2 shows the appearance of various types of stroke and normal brain tissues as seen on a CT scan. The diagnostic strategies of ischemic and hemorrhagic stroke differ in principle and often the treatment of one may prove fatal for the other. Hemorrhagic stroke often requires addition of coagulating agents in the blood in order to stop blood flow through the damaged artery where as ischemic infarct requires addition of blood thinning agents to increase the blood flow through the blocked artery. Hence correct identification of stroke type is necessary in order to proceed with the appropriate diagnosis and an automated stroke identification system could prove really helpful to the radiologists. Also, the main treatment for ischemic stroke requires the use of intravenous (IV) recombinant tissue plasminogen activator (t-PA), which if given in the early hours results in improved outcome. The t-PA is not a benign drug and increases the risk of hemorrhage by 10 times; hence it is only administered in cases where a substantial amount of recovery is possible. In Ischemic stroke cases, the amount of salvageable tissue becomes negligible (with respect to the risk offered by t-PA) after 4-6 hrs. from the onset of symptoms which makes the detection of early infarct of utmost clinical importance.

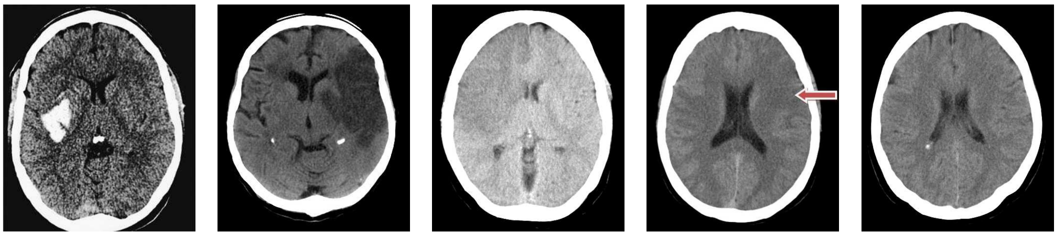

(a) Hemorrhage (left center) (b) Chronic (right center) (c) Acute (left top half) (d) Hyperacute (e) Normal

Figure 1.2 Representation of various types of stroke and normal brain

1.1.3 Imaging the Brain

Hosts of imaging technologies have been invented in order to non-invasively produce images of the internal organs of the body usually through altering the physical and chemical environment of the concerned body part. Some of the most widely used imaging technologies are Computed Tomography (CT), Magnetic Resonance Imaging (MRI), Positron Emission Tomography (PET) and Single-Photon Emission Computed Tomography (SPECT) (Figure. 1.3). CT and MRI provide physical imaging of the brain whereas PET and SPECT offer a way for imaging the physiological and functional aspects of brain. Out of these, CT and MRI are mostly used in the identification of Stroke and are discussed in more detail in the following sections.

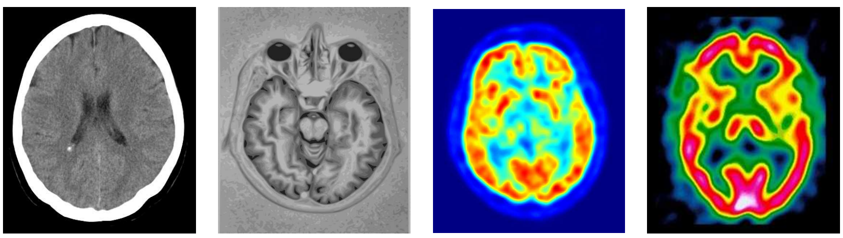

(a) CT (b) MRI (c) PET (d) SPECT

Figure 1.3 Representation of brain under various modalities

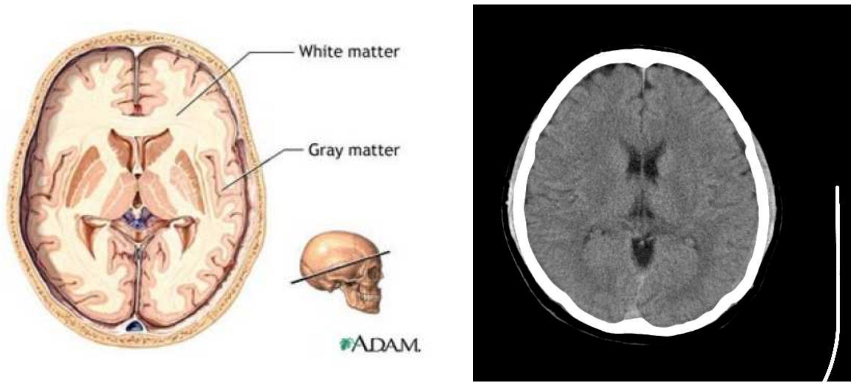

(a) Gray white matter on Atlas [38] (b) Gray white matter on CT

Figure 1.4 Tissue definition on CT

MRI makes use of Nuclear Magnetic Resonance (NMR) property to provide a detailed image of the internal organs of the brain. The technique requires first aligning the magnetization of the water molecules in the body using a powerful magnet followed by the disturbance of their alignment using a radio-frequency (RF) wave. After this the RF wave is turned off and the water molecules then slowly begin to move towards their initial alignment. During this re-alignment, the water molecules release their excess energy in the form of a signal which is then recorded by a scanner and transformed into an image. As seen from figure (Figure. 1.3(b)), MRI provides a very detailed image having good contrast between various types of tissues. MRI in form of Diffusion Weighted Imaging (DWI) is highly sensitive to stroke lesions and can be used to detect ischemic infarcts at a very early stage whereas the same cannot be said of CT images. Also unlike most other modalities, MRI does not require any ionizing radiation.

In CT, a series of x-rays are shot through the target region. These x-rays on passing through tissues get attenuated based on the characteristics on the tissues. Dense materials like bone exhibit larger attenuation compared to soft tissue like gray matter. These attenuated rays represent the projection profile of the tissues in their path and are caught by the x-ray detectors positioned around the circumference of the scanner. The above projection profile is taken from various angles and then mathematically combined to get attenuation profile of the target tissue. The attenuation profile of the tissues is measured in Hounsfield (H.U.) units. Table. 1.1 shows the attenuation values of common substances found in human body. In CT scans, higher H.U. corresponds to higher intensity and thus bony structures ($\geq$ 1000 H.U.) appear brighter than tissues (20-35 H.U.).

Figure. 1.5 shows a complete CT scan of a normal brain. The bony structures appear brightest as they offer maximum attenuation. White matter offers relatively lesser attenuation compared to gray matter and thus appears brighter. Any abnormal changes in the chemical or physical nature of brain cause a change in the attenuation profile and thus can be seen on the CT scan. These abnormal changes are sometimes difficult to evaluate as CT offers very poor tissue definition. The problem is accentuated by the presence of noise and other imaging artifacts like partial volume effect, beam hardening, motion

Air	<-1000
Fat	-70 to -30
Water	0
White Matter	20-25
Gray Matter	30-35
Blood	60-100
Bone, Metal	>1000

Table 1.1 Hounsfield scale

artifact, etc. Poor tissue differentiation can be easily seen in Figure. 1.4 which shows the appearance of tissues on CT compared to their actual model. We can see that the major areas of gray/ white matter tissues can be identified though detecting the exact boundaries is very difficult. The CT produces scans with very high dynamic range (16-bit images) and must be subjected to linear intensity scaling techniques in order to see them on standard display monitors [15], [1]. This intensity scaling process is known as *windowing* and explained in greater detail in chapter 4.

1.1.4 Stroke in Brain CT

Hemorrhagic stroke is characterized by hyperdense tissues and thus appear brighter than the normal tissues in CT scans (Figure. 1.2). The hyperdensity is due to the presence of hemoglobin in the blood which has higher attenuation than normal brain tissues. The attenuation of the affected tissues change with passage of time as the chemical composition of the blood changes due to the formation of clot and tissue death. This change in attenuation is linear with respect to time, beginning with hyperdense tissues (due to blood hemorrhage) and ending as hypodense tissues with attenuation resembling that of cerebrospinal fluid. Ischemic infarct is characterized by hypodense tissues and appears darker than the normal tissues. The hypodensity however is too subtle in the early stages and the affected tissues exhibit properties similar to other hypodense normal tissues namely, white matter. During the early stage of ischemic stroke, the reduction in blood supply to the affected tissue region leads to increased absorption of water and electrolytes by the affected region. The increase in water density decreases the attenuation of the affected tissue and this makes them appear darker than normal tissue. In the first 0-4 hrs., around 2-4% increase in water content occurs, causing the hypodensity of affected tissues to decrease in the range $\sim$[2 - 8] H.U. Under standard window settings, this usually leads to a change of $\sim$1-2 gray shade value in the affected regions on standard display monitors. These changes are so subtle and when paired with the noise and other artifacts that appear on CT scans can be easily missed by the human eye. The visual change (dark appearance) increases appreciably in the later stages of stroke with passage of time (Figure. 1.2).

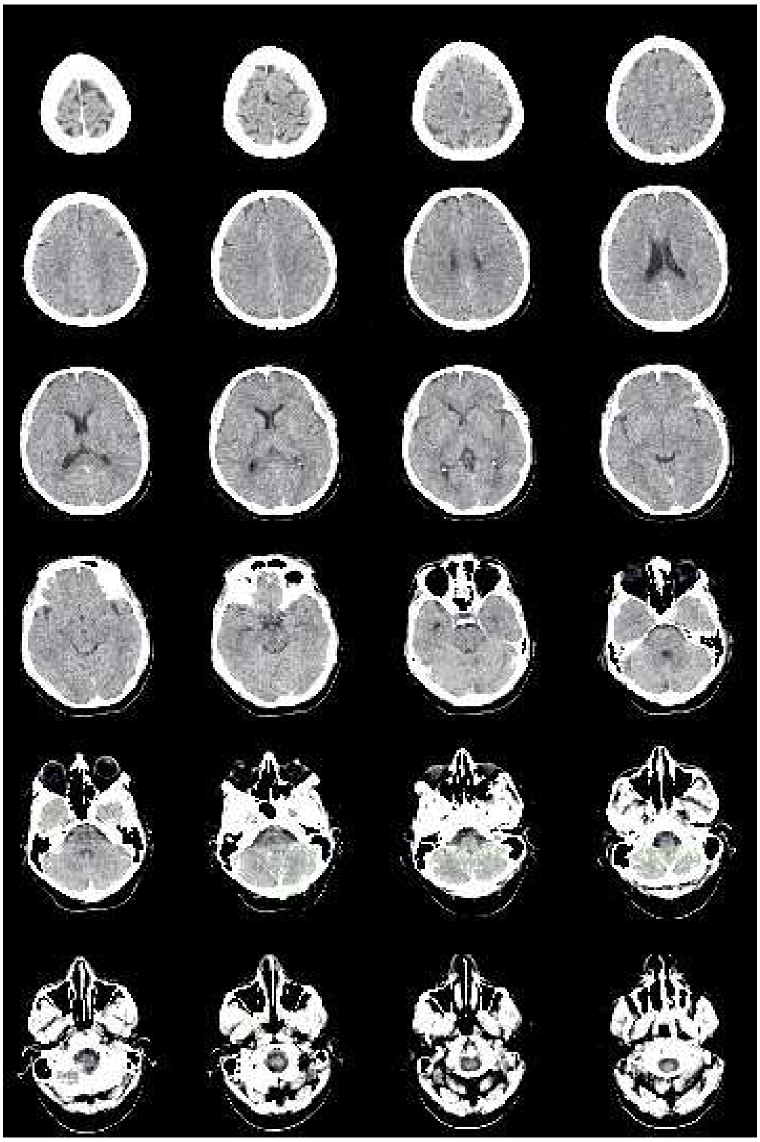

Figure 1.5 A volume CT scan of a normal brain

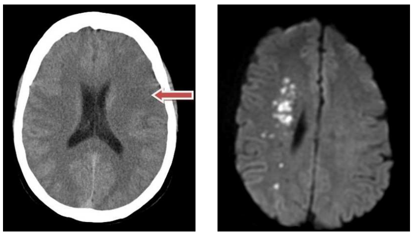

(a) CT (b) MR DWI

Figure 1.6 Appearance of early infarct on CT and MR

1.2 Why Unenhanced CT

Both CT and MRI are used extensively in the diagnosis of Stroke. MRI presents a better definition of stroke region especially in acute cases and as a result not much effort has been directed towards CT images (Figure. 1.6). However, the ground reality is that CT imaging is relatively quick, provides better spatial resolution and is more widely available than MR scanners in developing countries. In such countries, even when both scanners are available, CT imaging is the frontline modality used due to the cost differential in MR vs. CT imaging. Besides these major factors, other minor factor favoring the use of CT include the ability to also screen patients who are claustrophobic or have been inserted with surgical clips, metallic devices, cardiac monitors or pacemakers etc. Moreover, doctors around the world still perform CT as the first examination. This can be attributed to the fact that CT provides a better way of excluding conditions other than ischemic stroke which present similar symptoms but may require different treatment e.g. hemorrhages, infections, vascular malformations, etc. If the CT provides inconclusive evidence of ischemic stroke, further MR imaging is carried out in case it is available. Thus, until the availability and cost factors of the newer imaging modalities are improved, it is necessary to utilize the state of art research in imaging analysis in order to maximize the efficiency of radiologists for ischemic stroke detection from CT scans.

1.3 Earliest Visible Signs of Acute Infarct

In order to increase the detection accuracy of ischemic infarct during the first 0-4 hours, a lot of work was done to document the earliest visible changes on CT scans. These changes include loss of gray matter-white matter differentiation owing to decreased blood flow, ex. hypoattenuation of insula, basal ganglia, etc. (Figure. 1.7). The presence of hyperattenuating artery possibly due to arterial thrombus is another sign of ischemic presence which can be seen as early as 90 minutes from the onset of symptoms [42], [41]. Unfortunately, even in normal cases, some of the arteries can appear hyperattenuating and thus the interpretation of this sign must be done carefully in light of other signs of ischemic infarct. In some cases, edema related abnormalities like narrowing of the sylvian fissure, loss of cortical sulci can appear with the onset of ischemic stroke. Although these signs are among the first to appear, their

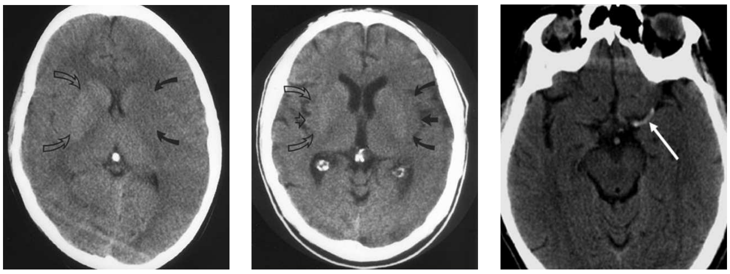

(a) Obscuration of lentiform nucleus (b) Insular ribbon sign (c) Hyperdense vessel sign

Figure 1.7 Various signs of early infarct [5], [40]

presence at the time of scan cannot be guaranteed. Nevertheless, these signs provide the only way of detecting hyperacute infarct during the ”therapeutic window” while also correlating with stroke severity. Moreover, experience plays an important role in identifying these signs due to their subtle nature [32]. Fiebach et al. [12] pointed out the importance of experience by demonstrating a significant difference in the performance of radiologists (more experienced) and neurologists (less experienced) in the case of CT interpretation as compared to MRI interpretation (which shows clear signs of early infarct). Their results supported the hypothesis that the ability to detect subtle signs of hyperacute infarct is dependent on the experience of the interpreter.

As mentioned earlier, the intensity change shown by the above hypodense changes are of the order $\sim$ [2 - 8] H.U., which under the standard soft copy viewing conditions [width 80 H.U., level 20 H.U.] represent a change of 1-2 gray scale levels. In order to accentuate these subtle signs, radiologists view the CT scan under non-standard window settings. The process involves viewing the concerned scan under a number of different window level settings at a reduced window width [$\sim$ 15 H.U]. The reduced window width increases the contrast between gray/ white matter tissues and enhances the subtleties of the ischemic signs. The increased contrast is accompanied by introduction of noise, artifacts, loss of tissue details, etc. and any decision-making requires careful thought. In spite of the enhancement achieved by reduced window width, some signs can be seen only under certain window level and while manually cycling through the different levels, the signs may be missed. The manual windowing process resembles a hit and trial procedure where initial training and experience of radiologists go a long way in determining the efficiency of its outcome.

Although the introduction of non-standard window settings have increased the detection accuracy of acute stroke from CT scans, it still fall short of the accuracy achieved by MR. This makes it necessary to devise automated CT analysis methods to accentuate the information available to the radiologists through automatic detection, enhancement, etc. Automatic detection of ischemic infarct is usually modeled on identification of one or more of the above mentioned signs. Identification of region specific signs like hypoattenuation of insula, basal ganglia, etc., requires automatic identification of those particular regions through some sort of brain template / atlas mapping, construction of which brings its own set of challenges.

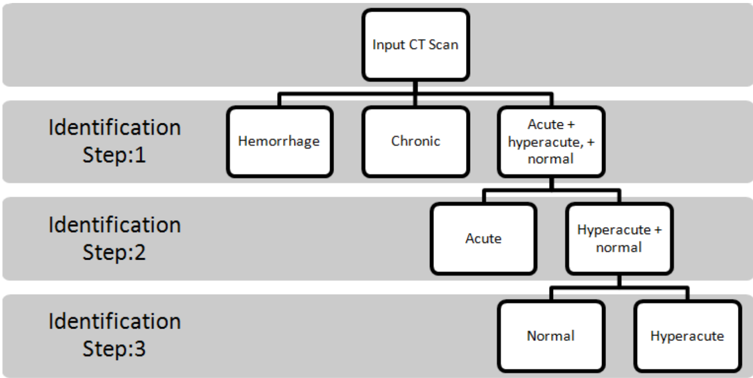

Figure 1.8 Automatic stroke detection framework

1.4 Problem Statement and Contribution

The aim of the thesis is the detection of stroke from brain CT scans during all stages of pathology, i.e. from the earliest possible stage (hyperacute) to the later (chronic) stages of infarction.

The thesis explores the stroke detection problem from two different point of views. The first track proposes a novel automatic stroke detection framework based on the characteristics of the abnormal tissue which presents the segmented stroke region to the radiologist. The second track aims at determining the best possible window-settings for a CT scan such that the perceptual difference between the normal and stroke-affected tissue is maximum. This makes it easier for the radiologists to manually locate the hyperacute infarct regions which can be missed by the automatic detection proposed in track 1. We will now explain the tracks in detail.

1.4.1 Track 1

The automatic detection algorithm uses the contral-lateral symmetry of the tissue distribution in brain to distinguish the stroke-affected tissues from the normal ones. The abnormality is modeled as a generic aberration in the otherwise contra-laterally similar distribution of gray/ white matter in the brain which enables us to identify early stroke signs without the use of atlas. Perfectly symmetrical strokes are a rarity and thus symmetry can be used as a powerful tool for its detection. The proposed algorithm uses a hierarchical scheme for stage-wise detection of stroke types on the basis of the loss in symmetry which characterizes each stroke type. Hemorrhage and Chronic infarct result in maximum symmetry loss and thus are extracted at first stage while the hyperacute infarct results in minimum symmetry loss and is extracted last. Figure. 1.8 shows the outline of the proposed framework.

Symmetry based detection of stroke requires a robust estimation of the mid-sagittal plane to divide the brain into left and right hemispheres. Our framework includes a novel symmetry plane identification method based on the physical features of skull. The method is much more robust than other prevalent methods which use the symmetrical distribution of brain tissue to locate the mid-sagittal plane. These methods perform well in case of normal brain but fail in cases where abnormality affects the symmetrical distribution of brain tissues.

1.4.2 Track 2

This track aims at increasing the efficiency of radiologists in detecting hyperacute infarct from CT scans by automatically finding the best possible window settings for viewing the particular CT scan. The auto-windowing of the CT scans is achieved through two different set of tissue properties namely, global (region-based) and local (pixel-based). The global method requires identification of candidate regions for presence of infarct and then the window parameters are determined based on the intensity characteristics of these regions. The second windowing approach, based on local tissue properties, is proposed as the region based method only enhanced those scans which it deemed abnormal. The result was that in scans where the approach missed the infarct, the scans were presented to the radiologists in unenhanced state, making them difficult to assess. The local approach removed this decision making on behalf of the algorithm and instead determined window parameters which maximized the disturbance in the tissue distribution of entire brain rather than from only the candidate infarct regions. It made sure that even in cases where the global method missed the infarct; the local approach would present the enhanced CT scan to the radiologist.

The detection of latter stages of infarct namely, acute and chronic, have more of a academic value for teaching radiologists where as hemorrhage and hyperacute infarct detection has more of a clinical value and can be used by radiologists during day to day clinical scenarios as shown by the experiments carried out in the later chapters. The next section would describe the layout of this thesis.

1.5 Thesis Structure

The structure of the thesis aims to present a stroke identification, detection and enhancement framework. The thesis is organized as follow:

- **Chapter 1 :** The Chapter deals with the introduction, objectives and contribution of the thesis.
- **Chapter 2 :** It gives a general background on the approaches already proposed by researchers on detection as well enhancement of different types of stroke.
- **Chapter 3 :** The chapter describes the automatic detection and identification framework. The dataset, validation methodology as well as the results are presented and discussed.
- **Chapter 4 :** The chapter presents two different approaches to find the best possible window parameters for manual detection of hyperacute infarct. A comparative analysis of the two methods is also discussed in the chapter.

- **Chapter 5 :** The final chapter deals with the discussion of the framework with respect to the results and presents a conclusion.

Chapter 2

Related Work

Stroke analysis is one of the most researched topics in Medical Imaging. A host of methods, both automatic and semi-automatic have been developed for detection, enhancement, segmentation etc. This chapter provides a summary of the research work done until now. In view of the methods presented in this thesis, which attack a number of problems, the literature survey has also been organized in a similar way. We will start our discussion from hemorrhage before moving on to ischemic stroke detection and finally ending the chapter with a summary of the methods developed for the contrast enhancement of the hyperacute infarct.

2.1 Hemorrhage Detection

Hemorrhage detection on CT has been a hotly researched topic in the field of medical image analysis in recent times. This can be attributed to fact that CT provides the best possible distinction between the normal and the affected tissue. The research was also encouraged due to the societal ramifications of hemorrhage whose patients tended to be typically 10 years younger than those of ischemic stroke. The approach in [8] exploits the fact that the hemorrhagic tissues are brighter than the normal tissues and initially uses a histogram-based k-means clustering followed by final segmentation using 3D morphological binary dilation of the initial clusters. The method also provides information about the growth of abnormal tissue by utilizing three sets of CT scan: within 3 hrs. after first symptoms, 1 hr. later, and within 20 hrs. after first symptoms. Majcenic et al. in [25] proposed an MRF-MAP based approach for segmentation of abnormal regions. In this method, the segmentation problem is treated as a pixel labeling problem and the optimal configuration is found by iteratively minimizing the energy of the configuration using an energy function. The method assumes the normal and abnormal tissues to be belonging to two different modes of histogram. Knowledge based approaches have been proposed in [6] and [4]. An unsupervised fuzzy clustering and expert system-based labeling of pixels is performed in the former while thresholding and morphological operations are done to segment candidate regions in the latter. The hemorrhagic candidates are then subjected to a knowledge based classification system that makes use of various image and anatomical features to separate the artifacts from the detected hemorrhagic candidates. A more comprehensive review of other methods for hemorrhage analysis can be found in [31].

Most of the research though, has been encouraged from the point of view of diagnosis of hemorrhage; as a result the work focuses more on accurate segmentation and volume quantification of affected tissue. Even though the current approaches may be modified to include provisions for automatic detection of hemorrhage affected scans, the area has not got much specialized attention. The detection process forms a key part of an automated ischemic stroke framework as only after the exclusion of hemorrhagic cases can the stroke treatment be made available to the patients. More recently, wavelet-based texture analysis has been used to first eradicate all the nasal cavity slices followed by intensity based thresholding [24] to detect the stroke-affected slices. Li et al. [23] proposed a knowledge based classification approach for obtaining the hemorrhagic regions from the non-brain tissues obtained from fuzzy C-means clustering followed by entropy based thresholding. All these approaches perform appreciably mainly because of the contrast between the appearance of hemorrhagic and normal tissues. The main reason for proposing a fresh approach for detection of hemorrhage was to develop an approach which would fit seamlessly with overall ischemic stroke detection framework and focused more on the presence of hemorrhagic tissues than on identifying or segmenting them.

2.2 Ischemic Stroke

Research on detection of ischemic stroke from CT scan was not as encouraging as that of hemorrhage. This can be attributed to a number of factors like poor tissue contrast provided by CT, noise and other imaging artifacts. Moreover the research avenues were further blocked due to the arrival of newer imaging technologies likes MRI which presented excellent potential in detection of early infarct. Maldjian et al. [26] proposed an atlas based acute infarct detection method. The brain atlas was used to first segment out the anatomical regions namely, right and left lentiform nucleus (globus pallidus plus putamen), internal capsule, and insula. These regions were then compared statistically with their contra-lateral counterparts based on their intensity histograms to detect any loss in symmetry. Matesin et al. [27] proposed a rule based approach to classify the different kinds of regions obtained by region growing. The method uses mid-sagittal plane which was detected automatically using center of mass of skull. Ušinskas et al. [44] proposed a texture features based approach to segment the ischemic infarct affected regions. The method utilized features such as mean, variance, histogram and gray level co-occurrence matrix to distinguish the normal tissue from the affected ones. Methods proposed by [44], [27] and many others assume that the normal and stroke affected tissues exhibited a sufficiently discriminating characteristics like tissue intensity, mean, various etc. The assumption is valid only in case of older infarcts which explains the poor performance of these algorithms when dealing with the early infarct whose detection is really important from diagnostic point of view. Moreover, as we have already discussed in earlier chapters, during the early stages of infarct the affected tissues mimic the characteristics of the normal tissues and therefore will be very difficult to detect without using some form of contra-lateral symmetry. Most of the methods avoid using the symmetry constraint and thus are difficult to modify so as to incorporate the early infarct detection. More recently, early infarct detection was attempted using shape information in [17]. Here, a probability measure based on average cohesive rate (a measure of spatial distribution of suspicious pixels around the concerned pixel) for selected pixels on both sides of the brain is used to assign likelihood of the presence of stroke. The method works for early infarct detection although the presence of a large number of parameters makes it a rather trivial approach. Moreover the accuracy figures for determining the line of symmetry have not been provided on which the entire algorithm stands. In addition to the work on infarct detection, research has also been going on for assisting the radiologists by enhancing the information available to them. We will discuss these approaches in detail in the next section.

2.3 Ischemic Stroke Enhancement

Efforts have been ongoing to increase the detection accuracy of early infarct ever since the advent of soft-copy CT. The invention of soft copy CT scans presented the radiologists power to manipulate the scans to view selected information in isolation which was not possible in case of hard copy scans. It also opened up new research avenue for using state of art image processing algorithms to assist the radiologists in their decision making. Bendszus et al. [2] were one of the firstm to present a contra-lateral symmetry based algorithm in which a density-difference diagram was obtained by simple subtraction of intensity histograms of contra-lateral hemispheres. The density-difference diagram was used to highlight the pixels exhibiting the highest density-difference. The CT scans along with the highlighted pixels were then rated by the radiologists for presence of infarcts. This method, although providing improvement in acute infarct detection rates, doesn't take into account the natural asymmetry and spatial information in tissue distribution, misalignment of mid-sagittal plane due to patient orientation. The spatial information is necessary in order to counter the natural asymmetry in the distribution of tissues in normal brain. Lev et al. [21], as mentioned earlier, demonstrated the benefits of using non-standard window settings under clinical conditions. The study proved that the sensitivity and specificity of detection can be increased by accentuating the perceptual difference between white and gray matter which was achieved through manually adjusting the window level and center. Subsequent studies confirmed the benefits of using non-standard window settings and the radiologists were then trained for differentiating between the affected tissues and artifacts under the non-standard window settinds which tend to increase the noise and graininess of the scan.

Seeing the performance enhancement brought about by linear enhancement (non-standard window settings), attempts were also made at non-linear enhancement of CT scans. Fayad et al. [11] presented a wavelet based multi-resolution histogram equalization algorithm to automatically enhance the perceptual difference among various types of tissues. Although aimed at chest CT, it showed that a significant reduction in interpretation times can be achieved. The diagnostic sensitivity and specificity were lower than in conventional window settings as non-linear enhancements tend to introduce artifacts. A biorthogonal filter bank based on splines has been proposed in [34] for enhancing the suspected stroke region. This results in enhanced appearance for acute infarcts. An extension to hyperacute cases is based on data denoising and local contrast enhancement using wavelets [39] [33]. Another approach for enhancement of hypo-attenuation uses adaptive median filtering to enhance the gray-white matter interface [19]. Although non-linear enhancements increase the contrast between the normal and abnormal tissue appreciably, they also tend to introduce unwanted artifacts [20]. The detection accuracy is also hampered by inevitable changes in relative intensities of tissues which interfere with the decision making of the radiologists. Although the intensity changes also occur in linear enhancement, their effects have been minimized through extensive training by radiologists. One way of countering the errors can be through increasing familiarity with the concerned method but making it a standard like the current prevalent windowing process is too much of an ask. Therefore the best way to increase the detection rate of early infarct is through using the state of art techniques to automatically determine the best possible window settings.

Chapter 3

Automatic Stroke Detection

This chapter details the complete proposed hierarchical approach for detection and identification of stroke. Our method is based on approach used by doctors who detect abnormality by examining the dissimilarity between the left and right hemispheres of the brain. The method of comparison used depends on the amount of asymmetry exhibited by the particular stroke type, for example, chronic and hemorrhagic infarcts can be detected by comparing the shape of their histograms whereas acute and hyperacute require much more complex symmetry comparison techniques. Figure. 1.8 gives an overview of the framework discussed in this chapter. In the first level, L_1 , a given slice is classified as belonging to one of 3 classes: L_{11} chronic infarct, L_{12} Hemorrhage and L_{13} normal, acute or hyperacute infarct. In the second level, L_{13} is split into two subclasses: L_{21} acute infarct and L_{22} containing normal and hyperacute infarct. The third level further separates L_{22} into two subclass: L_{31} hyperacute infarct and L_{32} normal. We will now describe the details of the proposed algorithm.

The proposed algorithm has three main steps. In the first step, the given slice is enhanced and denoised. Next, the line of brain symmetry is determined and finally, the abnormal slices are detected hierarchically.

3.1 Preprocessing

Since the dynamic range of the Hounsfield unit (H.U.) values for CT images is very large (-1000 to +1000 H.U.), the first task is to select the appropriate range of gray level for extracting soft tissue regions. The relationship between gray level (I (x, y)) and H.U. given as:

$$HU = I\left(x, y\right) + intercept \tag{3.1}$$

Where, the *intercept* value can be obtained from the meta information available in the DICOM header of CT volume data. The histogram of a given slice (Figure. 3.1(b)) consists of two major peaks corresponding to the background and soft tissue pixels. Since the H.U. values of the soft tissue are higher than that of the background (air), the higher intensity peak will correspond to the soft tissue region. A windowing operation to stretch the contrast is performed with the above peak value (P) as the

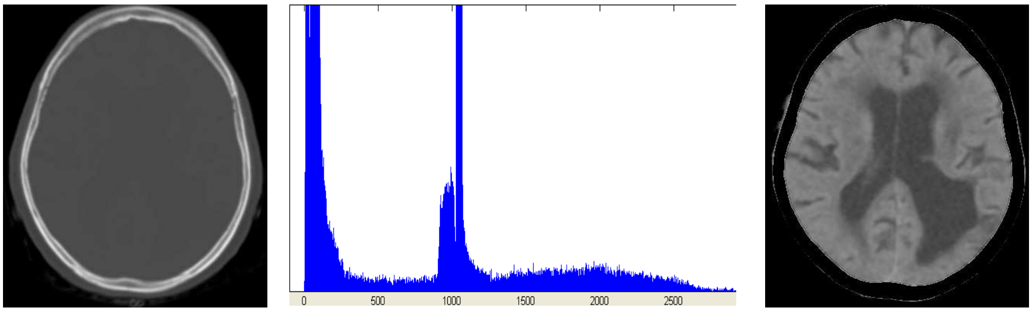

(a) Original image (b) Histogram of original image (c) Enhanced image

Figure 3.1 Preprocessing results

center and W (set to be 120 H.U.) as the width of the window:

$$I_{new}\left(x,y\right) = 255 * \frac{I_{original}\left(x,y\right) - \left(P - \left(\frac{W}{2}\right)\right)}{W} \tag{3.2}$$

After windowing, noise removal is performed using Wiener filtering to remove the graininess from the image. A sample image and the result of the enhancement and the denoising are shown in Figure. 3.1.

3.2 Mid-Sagittal Plane Detection and Rotation Correction

Since our approach is to compare the symmetry of the two hemispheres, it is necessary to correctly identify the mid-sagittal plane (MSP) or the line of symmetry. The physical structure of the skull is used to detect the rotation angle as well as the line of symmetry. A lot of other approaches have been designed to find the MSP which use the tissue symmetry to obtain the MSP. We use the physical structure instead of the tissue symmetry as our approach will be mostly required to find the MSP on the stroke affected cases where the tissue symmetry is already disturbed. There may be some cases, especially of hemorrhage where the physical structure of the skull itself gets deformed due to accident etc. Even in those cases, our approach might be able to find the MSP given that the nose portion of the skull is still intact.

The line of symmetry l_s is one that passes through the tip of the nose and bisects the horizontal line l_h passing roughly through the middle of the slice. We correct for any rotation present before extracting these lines. To find l_s we first search a set of slices (with high number of connected components) around the nasal cavity region. A sub-region is identified in these set of slices by locating the tip of the nose via a simple raster scan. The sub region is of size 30 x 512 and its horizontal projection profile is computed for every slice. The troughs in the profiles are found in either direction starting from the nose tip for each of the candidate slice. The slice which shows the steepest curve is chosen to be appropriate to detect and correct for rotation.

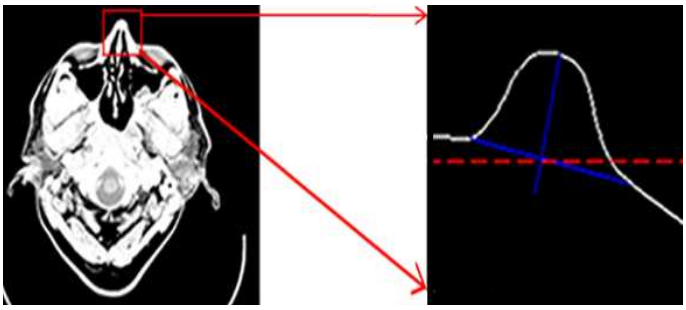

Figure 3.2 Nose extraction

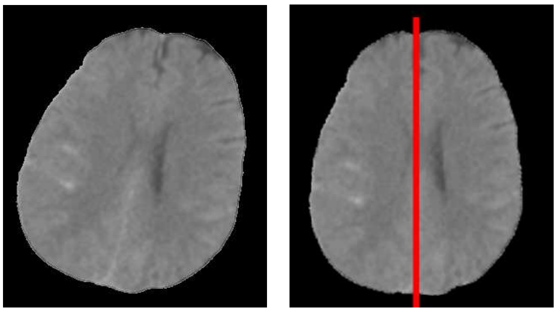

(a) Original image (b) Corrected image

Figure 3.3 Rotation correction results

In the axial view, the nose appears as a hill with the tip being the peak of the hill and the base being bounded by knee points of the hill (Figure. 3.2). In the absence of rotation, the line passing through the tip of the nose should be orthogonal to the line connecting the base of the nose. The knee points are easily detected by determining the rate of change of the slope of the nose boundary starting from the nose tip. The deviation of the base line from the horizontal gives the rotation angle which is used to perform a correction. This preceding step can only correct for rotation in the x-y plane. It is possible that the CT volume is also rotated in the axial direction (along the Coronal plane) which will mean the plane of symmetry will not be perpendicular to the x-y plane. Consequently, the lines of the symmetry for each slice will not align. In order to address this problem, we determine l_s for each rotation-corrected slice as follows: l_h is of same width as the horizontal projection profile of each slice and thus the required l_s is the bisector of l_h. A sample slice image and the result of rotation correction are shown in Figure. 3.3. The approach works good for cases showing a small amount of rotation ($\sim 10^{\circ}$ - 15 $^{\circ}$). Higher values of rotation makes the detection of tip of nose through raster scanning difficult as the first pixel that gets encountered is of the skull instead of the tip.

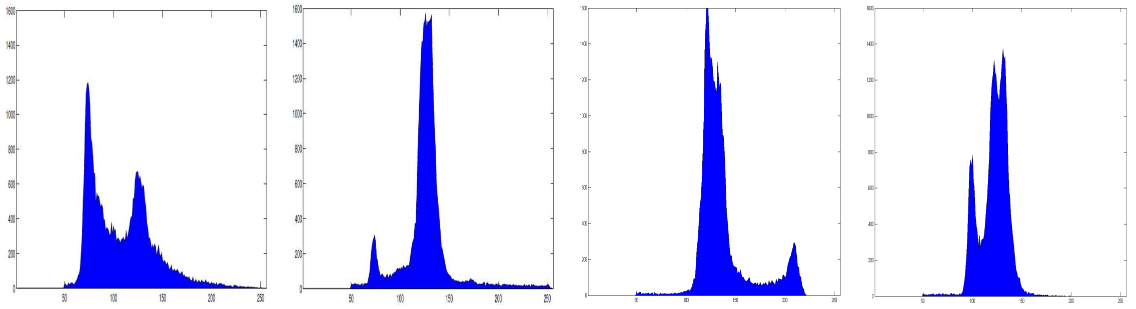

(a) Chronic affected histogram (b) Corresponding normal histogram (c) Hemorrhage affected histogram (d) Corresponding normal histogram

Figure 3.4 Histograms obtained at level 1

3.3 Stroke Detection and Identification

The detection algorithm performs a 3-level classification to identify abnormal and normal slices. Histogram features are used in the first level while wavelet-based features are used for the second level. In the third level, due to subtle nature of hyperacute infarct, rough gray/ white matter segmentation is performed using Markov Random Field (MRF) and then their distributions in the two hemispheres are compared spatially. The following sections describe each level of the framework in detail.

3.3.1 Level 1 Classification

The first step differentiates the encephalic slices into three classes L_{11}, L_{12} and L_{13} as described earlier, based on their histogram features. The l_s information is used to divide a slice into two hemispheres and the histogram for the right and left hemispheres are computed and compared for similarity. The similarity metric used is the correlation coefficient which is computed on a subsampled (by 5) version of the 2 histograms. The histograms of left and right hemispheres exhibit significant difference in the lower intensity bins (50-100) in case of chronic infarct whereas for hemorrhage the difference is observed in higher intensity bins (200-250) (Figure. 3.4). Since only the low and high indexed bins are of interest, the measure is computed only for those bins. If this measure is below a threshold the corresponding bin number is noted. If the bin number is low, the slice is classified as belonging to L_{11} and if the bin number is high the slice is classified as a member of L_{12}. If the measure is below the threshold in both low and high indexed bins, the implication is that both type of abnormalities present in the slice. Therefore such slices are accorded membership in both L_{11} and L_{12}. All the remaining slices are classified as belonging to L_{13}.

3.3.2 Level 2 Classification

In the second level of classification, the goal is to differentiate between normal and acute infarct cases. Histogram features are insufficient for this purpose as their gray value distributions overlap. This

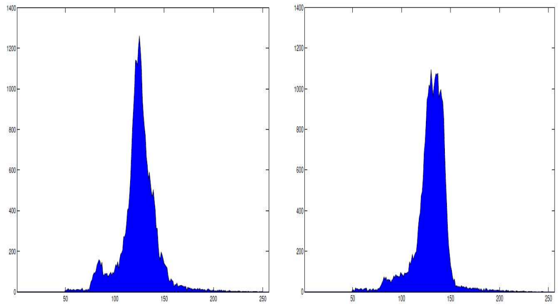

(a) Acute infarct affected histogram (b) Corresponding normal histogram

Figure 3.5 Histograms acute infarct

can be seen from the histograms shown in Figure. 3.5. Since the difference between the distributions is subtle, a finer analysis is required. A wavelet decomposition of the histograms is employed for this analysis. Daubechies-4 wavelet decomposition up to 5 levels is used to compute the energy distribution in the scale space. The corresponding energy values of the two histograms are compared using a simple difference of energy measure. If the difference is above a threshold, the slice is classified as belonging to L_{21}. All other cases are classified as normal (L_{21}).

3.3.3 Level 3 Classification

The third level classification deals with the detection of hyperacute infarct. During the time frame of hyperacute infarct (0-4 hrs.), very subtle changes occur in the affected tissues. These include blurring of gray/ white matter junction, hyperattenuation of blood vessels, edema related abnormalities etc. All these indicators affect the distribution of gray/ white matter in the left and right hemispheres, but accurate separation of brain tissues into gray/ white matter is very difficult owing to the poor tissue contrast and noise offered by the CT images. As a result most of the tissue classification methods require some sort of additional knowledge in the form of different modality images, etc. An example is [48] which uses multimodal information from PET/CT pairs to boost the classification. In order to overcome these limitations, we propose to a novel approach that uses rough segmentation of brain tissues. The aim of the approach is to achieve a best possible segmentation of gray/ white matter and then use a symmetry measure which negates the inaccuracies in the tissue segmentation.

Although work on tissue classification in CT is limited, it is a widely researched problem in brain Magnetic Resonance (MR) images. Most of these methods employ probabilistic models ([30], [10], [49] etc.) for tissue classification as these models provide an effective way of incorporating spatial information and are generally resistant to noise. In our method, we propose an automatic segmentation of brain CT images by using MAP-MRF model [14] which combines the Markov random field (MRF) and the maximum a posteriori (MAP) approach for classification. Such an approach has been adopted

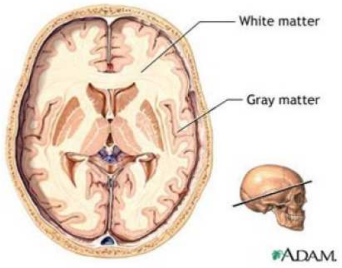

(a) Gray/ white matter on Atlas

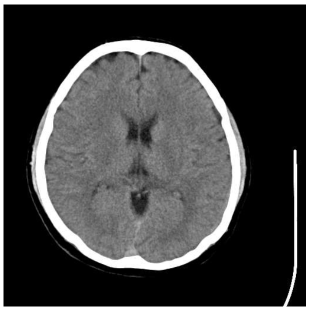

(b) Gray/ white matter on CT

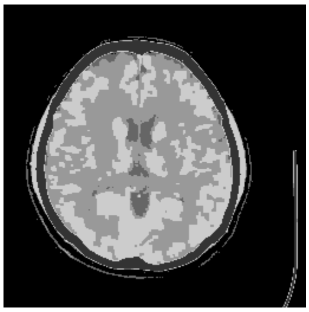

(c) Rough segmentation

Figure 3.6 Rough segmentation of gray white matter on CT

for PET/ CT pairs [48] but not for CT exclusively. The next section explains the representation of a CT image using MRF model.

MRF Model

We assume that images are defined over a finite lattice S = $\{S_i,\ 1 \leq i \leq N\}$ where S_i denotes the pixels. The notation S_i and subscript i are interchangebly used to demontrate the same location S_i. For each pixel S, the class to which the pixel belongs is specified by a class label, L_i, which is modeled as a discrete random variable L = $\{L_i,\ 1 \leq L_i \leq M\}$. We are also given an MRF on these units, defined by a graph G (where the vertices represent the units, and the edges represent the label constraints of the neighboring units), and the clique potentials. Let c denote a clique of G and Ω the set of all cliques of G.

In MRF theory, a configuration refers to a state where each site S_i belongs to a particular label L_i. Our goal is to find the best possible configuration L (L $\in \Psi_L$, where Ψ_L represents the configuration space), which maximizes the posterior probability of L. The posterior probability is given by

$$P\left(L|S\right) \propto P\left(S|L\right)P\left(L\right) \tag{3.3}$$

Imposing an identical, independent Gaussian distribution for the voxel values at each targeted region in the given image, we have

$$P(S|L) = \prod_{1 \le i \le N} P(S_i|L) = \prod_{1 \le i \le N} P\left(S_i|L_i\right) \tag{3.4}$$

and,

$$P(S_i|L_i) = \frac{1}{\sqrt{2\pi}\sigma_{L_i}} \exp\left(\frac{\left(S_i - \mu_{L_i}\right)^2}{2\sigma_{L_i}^2}\right) \tag{3.5}$$

where μ_{L_i} is the mean and σ_{L_i}, is the standard deviation of class L_i. The prior model, P(L) can be assumed to follow Gibbs distribution [16] given by,

$$P\left(L\right) = \frac{\prod_{c \in \Omega} exp\left(-E_c\right)}{Z} \tag{3.6}$$

Where E_c refers to the energy of the configuration and Z is a normalization factor. Combining equations 3.3, 3.4 and 3.6, we have for the posterior probability,

$$P\left(L|S\right) \propto \prod_{1 \le i \le N} P\left(S_i|L_i\right) \prod_{c \in \Omega} exp\left(-E_c\right) \tag{3.7}$$

It is further assumed that the configuration field L is a second order MRF [22] which gives the prior model as (using equation. 3.6),

$$P(L) = \frac{1}{Z} \exp\left(\frac{-1}{T} \sum_{\{S_i, S_j\} \in \Omega} \beta V\left(L_{S_i}, L_{S_j}\right)\right) \tag{3.8}$$

Where T is the temperature, Ω is the set of second order cliques, β is a model parameter controlling the homogeneity of regions and V(L_{S_i}, L_{S_j}) represents the second order clique potential, defined as

$$V(L_{S_i}, L_{S_j}) = \begin{cases} 1, \text{ if } L_{S_i} \neq L_{S_j} \\ -1, otherwise \end{cases} \tag{3.9}$$

The estimate of L denoted by $\hat{L}$, global energy, (E$_{glob}$(L)) and the local energy (E$_i$(L) at site S$_i$), are determined following the method in [3]:

$$\begin{aligned} \hat{L} \;=\; & argmin_{L \in \Psi}\left(\sum_{1 \le i \le N} \left(F\left(i\right)\right)\right. \\ & \left. + \frac{1}{T} \sum_{\{S_i, S_j\} \in \Omega} \beta V\left(L_{S_i}, L_{S_j}\right)\right) \end{aligned} \tag{3.10}$$

$$
\begin{aligned}
E_{glob}(L) &= \left(\sum_{1 \le i \le N} (F(i)) + \right. \\
&\left. \frac{1}{T} \sum_{\{S_i, S_j\} \in \Omega} \beta V\left(L_{S_i}, L_{S_j}\right) \right)
\end{aligned} \tag{3.11}
$$

The local energy at site S_i is the energy of the site in isolation, given by $F(i)$ and the energy of the neighbourhood (Ω_i) cliques.

$$
\begin{aligned}
E_i(L) &= F(i) + \\
&\frac{1}{T} \sum_{\{S_j, S_k\} \in \Omega_i} \beta V\left(L_{S_j}, L_{S_k}\right)
\end{aligned} \tag{3.12}
$$

Where F(i) represents,

$$
F(i) = \frac{1}{T} \left(\log \sqrt{2\pi} \sigma_{L_i} + \frac{\left(S_i - \mu_{L_i}\right)^2}{2\sigma_{L_i}^2} \right) \tag{3.13}
$$

The segmentation process which minimizes the above mentioned energy requires the initialization of the distribution parameters (mean, variance) of all the label classes. These parameters can be estimated using various methods such as histogram analysis, maximum likelihood estimation, thresholding etc. Since the estimation of distribution parameters influence the performance of the segmentation algorithm, we want to partition the pixels into classes such that the interclass variability is maximum which is achievable using Otsu's method of segmentation [28]. We perform Otsu segmentation to classify the brain pixels into M (=2) classes namely, white and gray matter. We need only two classes as after the preprocessing only the soft tissues are left. Once the classes are determined, the distribution parameters namely, mean and variance are calculated and provided to the energy minimization algorithms for further estimation.

The poor tissue contrast in CT will weigh down the performance of the segmentation algorithm. We seek to address this by increasing the contrast between the various tissue classes *prior* to their segmentation. The pipeline of processing for our proposed method is shown in Figure. 3.7. As indicated, the processing is carried out at the slice level in the first two stages as well as in the probability map generation step. Midline detection and the final decision on the presence of infarct are done at the volume level. The complete pipeline is described in detail next.

3.3.3.1 Contrast Enhancement

Since only soft tissues are of interest, the first step is to extract the brain tissues which lie in the range of white/gray matter (16-50 H.U) which results in stripping of skull, etc which lie outside the tissue

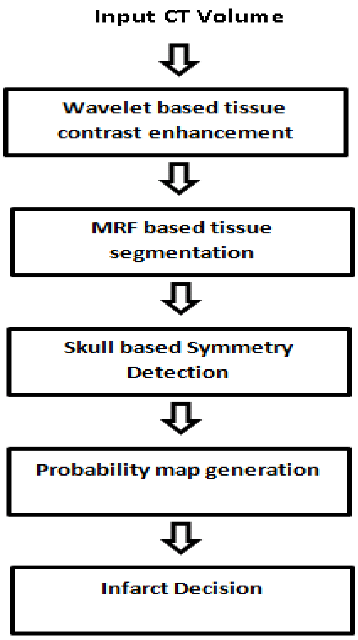

Figure 3.7 Algorithm outline

range. These tissues are then enhanced using a method very similar to [7]. A CT slice is decomposed into four frequency sub-bands using Daubechies_9 wavelet to extract the illumination information of the image. The illumination sub-band is then equalized, based on the intensity profile of the same slice with modified window settings using singular value decomposition (SVD). The singular value matrix obtained after SVD contains only the illumination information and hence modifying it results in preserving other important details (Figure. 3.8(a)).

3.3.3.2 Tissue Segmentation

The tissue segmentation involves maximization of the posterior probability of the MRF model which we calculated in the previous section. This is done using Modified Metropolis Dynamics (MMD) as it is generally faster and provides a lower energy output when compared with other optimization techniques [3]. MMD involves the following steps:

1. Pick up randomly an initial configuration L0, with iteration k=0 and temperature T=T_a (where T_a is a constant).

2. Pick a global state L' such that: 1≤L'_i ≤M and $L'_i \neq L^k{}_i$, 1≤i≤N, Where k refers to the iteration number.

3. For each site Si, the local energy E_i(L'), where L' = ($L^k{}_1,\ldots,L^k{}_i,\ldots,L^k{}_N$) is computed using equation 3.12.

4. Compute ΔE$_i$ = E$_i$(L') - E$_i$(L^k), the new label at site S$_i$ is accepted if if ΔE$_i \leq 0$ or $\alpha \leq \exp\left(\frac{-\Delta E_i}{T}\right)$ where $\alpha \in$ (0,1) is a constant.
5. Decrease the temperature T (k+1) = a $\times$ T (k) (where a = 0.9 is a predefined constant, used to control T and $T(0)$=4) and go to step 2 until the number of modified sites is less than a threshold.

To aid convergence of the algorithm, the entire image is first partitioned into disjoint regions R$_n$ (1$\leq$n$\leq$2). This initial segmentation is carried out by assigning a label to each pixel which generates the least amount of Gaussian energy (using log of equation 3.5). The tissue segmentation results in a binary map with white matter indicated in black (Fig. 3.8(b)).

(a) Enhanced image (after skull stripping)

(b) Extracted binary image

Figure 3.8 Extraction of hypodense pixels.

3.3.3.3 Candidate Selection

Candidate affected pixels are identified based on contra-lateral symmetry of a slice. The left and right hemispheres of a brain appear symmetric but are similar at best. Many small discrepancies exist even in the normal brain [47] which can unfavorably affect any attempt to detect abnormality (like stroke) based on global contra-lateral symmetry. These discrepancies, unlike stroke, seldom continue across the slices (in axial direction) due to considerable thickness of the slices. Hence, the symmetry is assessed in a 3-dimensional neighborhood (which is a $n \times n \times$ 3 (slices) window, W) of every hypodense pixel in both the hemispheres and an abnormality measure P (-1 $\leq p \leq$ 1) is defined as follows.

$$P_{S_i} = \frac{\sum\limits_{W_{S_{iRight}}} S_{iRight} - \sum\limits_{W_{S_{iLeft}}} S_{iLeft}}{3 \times n^2} \tag{3.14}$$

Where, S$_{iRight}$ and S$_{iLeft}$ refer to corresponding pixel locations. Deviation of P from 0 (symmetry state) gives the measure of asymmetry in the distribution of hypodense tissues in the vicinity of the concerned tissue and its counterpart in the other hemisphere. Any deviation from the symmetry state ('0') implies excess of hypodense pixels thereby indicating higher possibility of infarct. The value $|P_{S_i}|$, is

Dicom Tag	Information	Value
0008-0070	Manufacturer	Siemens
0008-1090	Model Name	Emotion 6
0018-0050	Slice Thickness	6 mm
0018-1150	Exposure Time	1000
0018-1151	X Ray Tube Current	240 μA
0018-5100	Patient Position	HFS

Table 3.1 CT acquisition protocol

the probability that S_i belongs to an infarct region. A higher value of P_{S_i} indicates greater discrepancies between the hemispheres at S_i and thus exhibiting higher probability of presence of infarction. The required candidates are found by applying a confidence threshold (determined empirically) to this map in order to account for the natural asymmetry present in the brain.

3.3.3.4 Hyperacute Infarct Region Detection

Given the set of infarct candidates, we impose spatial contiguity across slices to reject the false candidates. This is achieved by declaring only those regions which show significant overlap in neighboring slices as belonging to infarcts. The constraint helps in filtering out false positives which are detected by the algorithm as they exhibit a natural asymmetry in tissue distribution.

3.4 Results and Discussion

3.4.1 Dataset Details

The performance of the method has been tested on a dataset collected from a local hospital. A detailed acquisition protocol is given in Table. 3.1. The dataset consists of volume CT data of 42 patients. Out of these 19 were normal, 5 hemorrhagic, 6 chronic, 6 acute and 6 hyperacute. Since the time of scan was not available, the abnormal cases were classified into chronic, acute and hyperacute by the doctors based on the difficulty encountered while identifying the infarct regions. Follow up scans of these cases were collected and one expert's markings on these scans were used as the ground truth. The scans were from patients belonging to various age groups (7, 15, 20 datasets in the age-groups 0-30, 30-50, 50 and above respectively) to help in robust testing since natural symmetry is disturbed as the age advances. In abnormal cases, it was assumed that the number of affected slices remained the same in follow-up scans (i.e. no growth of abnormal tissue between subsequent scans).

Patients	Normal Cases 19	Abnormal Stroke Cases 23			
		Infarct			Hemorrhage
		Chronic	Acute	Hyperacute	
Slices (Groundtruth)	291	40	61	45	35
True positive	261	38	56	37	28
False negatives	30	2	5	8	7
False positive	22	4	8	16	2
Recall(%)	89.69	95.00	91.80	82.22	80
Precision(%)	92.22	90.47	87.5	69.81	93.3

Table 3.2 Results of the complete system at slice level

3.4.2 Detection Results and Discussion

The qualitative results of the algorithm are showcased in Figure. 3.9 and 3.10. Figure. 3.9 show the results of the MRF-based detection on a normal, acute and hyperacute dataset. The algorithm succeeds in picking out the affected regions but in the process it also picks up false positives (Figure. 3.9(d)). The reason being that the slice exhibits difference in tissue distribution in the lower side of brain which can be easily seen from the extracted tissue map (Figure. 3.9(c)). Such differences in distribution occur frequently in brain but fortunately the spatial contiguity constraint takes care of most of them. Figure. 3.10 shows the outcome of detection algorithm on two more hyperacute slices side-by-side with their corresponding follow-up CT scans. We can clearly see that the algorithm performs good as far as the detection of core area of infarct is concerned, however it fails to detect the periphery regions of infarct core as the symmetry disturbance in those region is not significant enough at the time of CT scan.

As discussed earlier, the detection of early infarct carries clinical value whereas the latter stages of stroke carry mostly an academic importance. This makes it necessary to present the results of our algorithm under both clinical and academic requirements. We therefore, showcase the results of the entire system as a whole, on the previously mentioned dataset (Table. 3.2) and also on a subset dataset (Table. 3.3) comprising only hemorrhage, hyperacute and normal cases. We also include the acute cases in this dataset as there is a fuzzy boundary between the hyperacute and the acute cases and it's very difficult to differentiate one from another. The performance on second dataset gives us a clearer picture about the performance of the algorithm under clinical conditions. Moreover, to gauge the performance of the entire approach with regards to separating normal and stroke (hemorrhage and ischemic) cases, we present the corresponding performance figures for the same in Table. 3.5 . Apart from the slice level results, we also present the patient level results (Table. 3.4) which gives true picture of the performance of the algorithm. Patient-level results give us additional information like number of affected patients that were declared normal, also the number of normal patients which were declared as affected. The former information is more important in case of medical imaging as the algorithm must ensure low false negative rate even at the cost of a relatively high false positive rate.

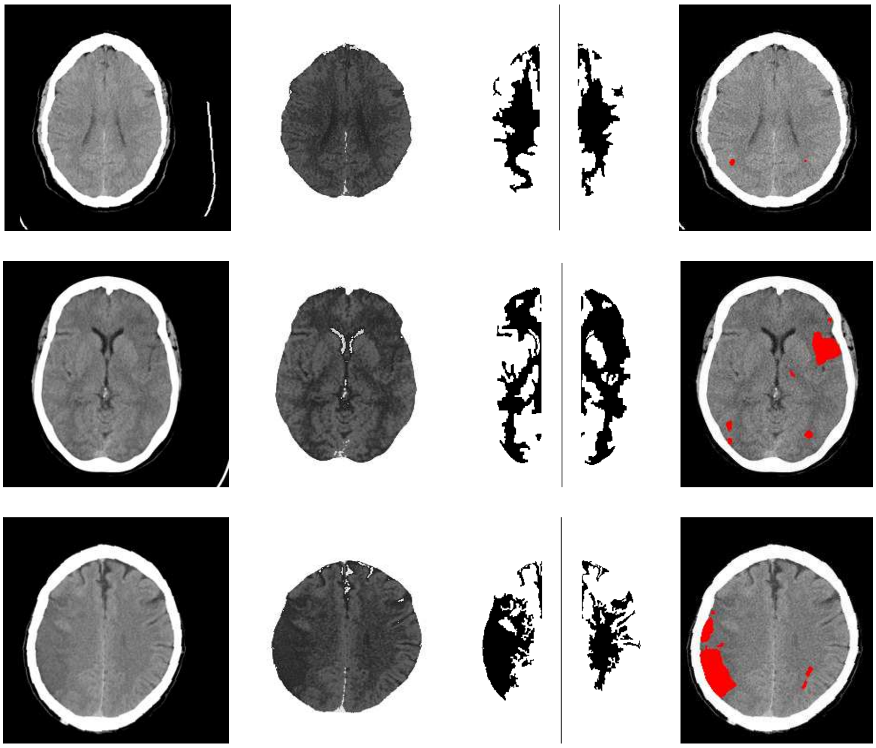

Figure 3.9 Results of proposed algorithm on normal, hyperacute and acute datasets (rows 1-3 resp.).The columns 1-4 depict input image, enhanced tissue region, extracted hypodense tissue and detected abnormality (overlapped on input image) resp.

Table. 3.2 shows the performance of the algorithm at slice level. The algorithm performs well in cases of chronic and acute infarct as is evident from the high precision and recall figures. The presence of a number of false negatives in these cases (2, 5 respectively) were mostly the boundary slices of the infarct where only a fraction of infarct is present and the disturbance in contra-lateral symmetry is not sufficient for detection. Figure. 3.11 shows the boundary slice of a stroke affected patient alongside a similar slice from a normal patient. As is clear from the figure, the tissue distribution in both the slices appear similar which causes the algorithm to miss the affected slice. Hyper acute detection figures are slightly lower than chronic and acute cases, with precision and recall rate being 69.81% and 82.22%. In spite of the lower precision rate, a higher recall rate showcases the efficiency of the algorithm under clinical conditions. The lower precision rate is mainly due to the slices in which the inherent symmetry of the normal brain is lost due to various reasons, for example, widening of sulci which can be seen in

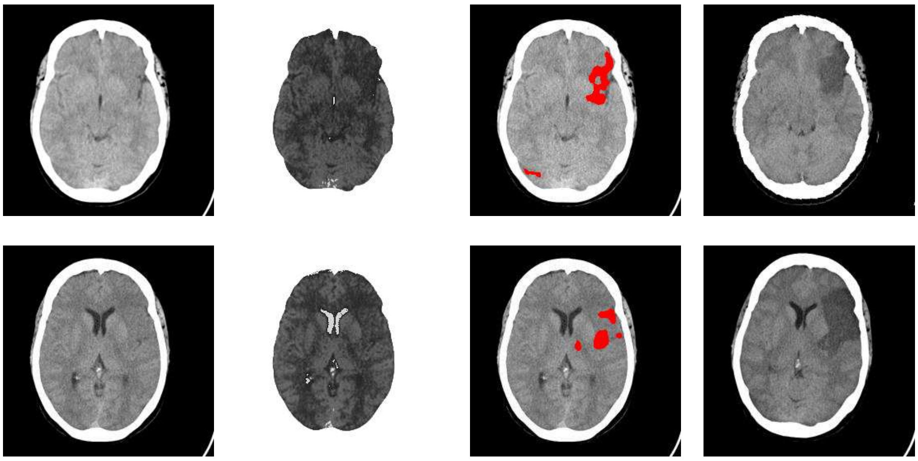

Figure 3.10 Results of proposed algorithm on hyperacute slices showing input image, enhanced tissue region, detected abnormal tissues, corresponding follow-up scan (in columns 1-4 respectively).

	Normal	Infarct	Hemorrhage
Patients	19	12	5
Slices	291	106	35
True Positive	261	93	28
False Negative	30	13	7
False Positive	20	28	2
Recall TP/(TP+FN)	89.69	87.73	80
Precision TP/(TP+FP)	92.88	76.85	93.33

Table 3.3 Results depicting clinical scenario

Figure. 3.11(b). Also, thicker slice reconstruction can result in partial volume effect which sometimes mimics the hypodensity observed in ischemic stroke and can be falsely picked up by the algorithm. Also a number of hyper acute infarct slices were missed by the algorithm, most of which were the boundary slices exhibiting the same problems as explained before. In some of the cases, the infarct might not have reached the particular boundary slices when the initial scan was conducted. Since we assume in the beginning that the number of affected slices remain the same between the initial and the follow-up scan. Since in our case, most of the follow ups were taken around 1-2 days after the initial scan, there is a possibility of growth of ischemic tissues due to complete infarction of the penumbra regions [13]. Therefore due to lack of sufficient condition we still consider missed slices when compared to follow up scans as false negatives which probably bring down the actual performance of the algorithm slightly. The algorithm also performs reasonably well in case of hemorrhage giving about 80% recall and 93.33% precision. The higher precision value is mainly due to the contrast in the gray values of hemorrhage (hyperdense) and normal brain tissues. Although, even in case of hemorrhage, various mural vascular calcifications can mimic hyperdense regions due to partial volume effect and in some cases are picked up by the algorithm as belonging to hemorrhage.

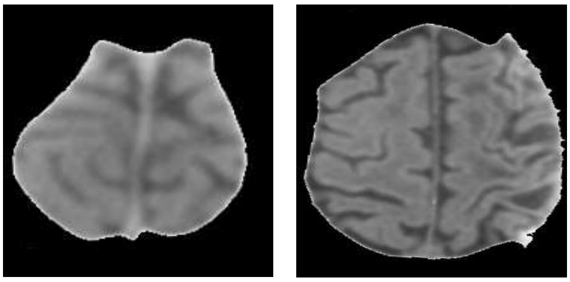

(a) Missed hyperacute slice (b) Normal slice

Figure 3.11 Comparison of missed hyperacute boundary slice with normal slice

Table. 3.3 showcases the performance of the algorithm on a subset of the original dataset comprising only of cases which have clinical importance i.e. hemorrhage, acute and hyperacute cases. In order to be useful in clinical scenario, the algorithm must first be able to separate the hemorrhage cases from the normal and hyperacute ones and then must be able to detect the hyperacute cases with high degree of accuracy. Our algorithm gives a recall rate of 80% and 87.73% in case of hemorrhage and early infarct (both acute and hyperacute) cases respectively. The recall rate of hemorrhage detection seems low indicating the shortcoming of the algorithm. The same is true of infarct detection but to a lesser degree. In spite of the lower performance, the numbers that really matter in clinical scenarios are the patient level results which show the actual number of affected patients that go through undetected by the system.

Patients	Normal Cases 19	Abnormal Stroke Cases 23			
		Infarct			
Patients (Groundtruth)		Chronic	Acute	HyperAcute	Hemorrhage
	19	6	6	6	5
True positive	18	6	6	5	5
False negatives	1	0	0	1	0
False positive	1	0	0	1	0
Recall (%)	94.73	100	100	83.33	100
Precision (%)	94.73	100	100	83.33	100

Table 3.4 Patient level results of the complete system

The patient level figures are shown in Table. 3.4. The figures indicate that even though the algorithm is not able to pick out all the affected slices, it does pick out a few in each affected case to mark them as affected. The algorithm gives 100% precision and recall in case of chronic, acute and hemorrhage. The slightly lower performance in case of hyperacute was due to inability of the algorithm to detect any stroke slice in a hyperacute case having a small infarct visible in just two slices. The presence of infarct

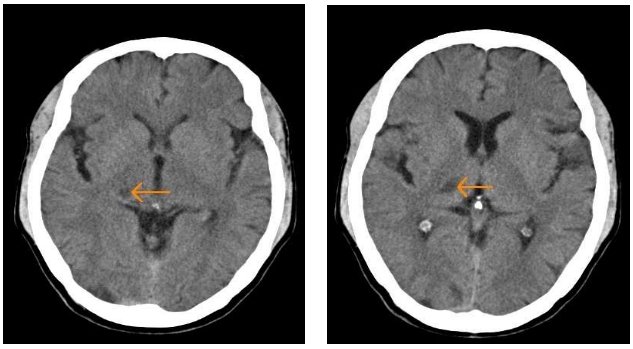

(a) Slice 1 (b) Slice 2

Figure 3.12 Hyperacute failure case (infarct indicated by arrow)

	Normal	Stroke-affected
Patients	19	23
Slices	291	181
True Positives	261	157
False Negatives	30	24
False Positives	22	30
Recall (%)	89.69	86.74
Precision (%)	92.22	83.95

Table 3.5 Table showing system level performance

in just two slices mimics the behavior of the typical asymmetry shown by the abnormal CSF distribution by the normal brain and is therefore classed as same. Figure. 3.12 shows the above referred case.

Finally, in Table. 3.5, we present the slice level results to gauge the performance of the system in a normal vs. stroke-affected (both ischemic and hemorrhagic stroke) scenario. In this scenario, our approach registered a high recall and precision rate (86.74% and 83.95% respectively) for detection of stroke on brain CT. The above tabulated results indicate a reasonable level of performance in case of hyperacute stroke which carries the maximum clinical importance. This encouraged us to look for alternate approaches for increasing the accuracy of radiologists in detecting early infarcts. The next chapter describes one such approach which aims at empowering the radiologists with more information to make their decision making as accurate as possible.

Chapter 4

Enhancement of Early Infarct through Auto-Windowing

As explained in previous chapter, automatic detection of hyperacute infarct from non-contrast CT is a very difficult task mainly because of the subtle developments which take place in the affected region which are often masked by the low tissue contrast and the noisy nature of CT scans. Clinically, detection of hyperacute infarct is of utmost importance and since the automatic detection rates were low, a different strategy was adopted to increase the accuracy of radiologist for hyperacute infarct detection.

The new strategy was inspired by the current detection method adopted by the radiologists in case of hyperacute infarcts and focuses on enhancement of infarct tissues rather than its automatic detection. The enhancement strategy can help the radiologists in clinical scenarios by making the infarct tissue easier to detect. The doctors currently use a manual windowing procedure to look for the various signs exhibited by the infarct tissues during the early hours of onset. In the coming sections we will first describe the windowing process before moving onto our automatic approach.

4.1 Manual Windowing

CT scans produce 16-bit images consisting of 65, 536 different grayscale values. Only a small portion of these grayscale values contain information useful for the radiologists, with the rest representing the attenuation coefficients of air, surrounding objects, etc. Windowing in medical images refers to selecting the required range of grayscale values out of the 65, 536 and mapping them to the display range of the monitor. Different chunks of grayscale values provide different information about the scan and windowing can help in looking at various different aspects of the CT like bones, soft tissue, etc. in isolation. Figure 4.1 gives a good idea of the windowing process.

Mathematically, Windowing is defined as a one to one mapping function between two sets of intensities, source intensities ($L_s \in L_{s1}$, L_{s2}, ..., L_{sm}) and the destination display intensities ($L_d \in L_{d1}$, L_{d2}, ..., L_{dn}). In case of medical imaging, the destination is the display monitor having intensity range $L_d \in (0, 1, 2, ..., 255)$. The range of source intensities is described in terms of two parameters, window width W_{width} and window center W_{center} such that,

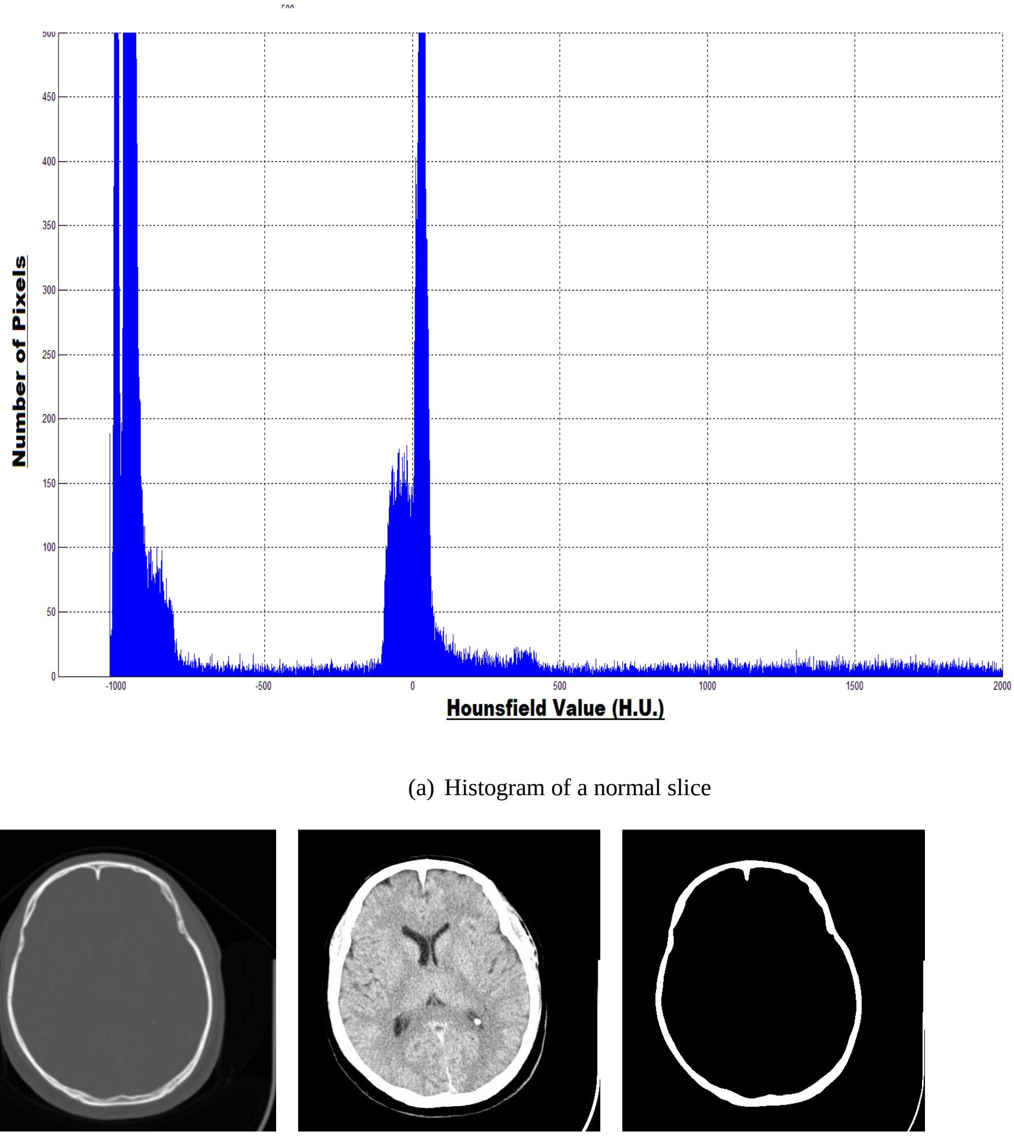

(a) Histogram of a normal slice

(b) Entire CT range

(c) Soft tissue range

(d) Hard tissue range (bone)

Figure 4.1 Demonstration of windowing process

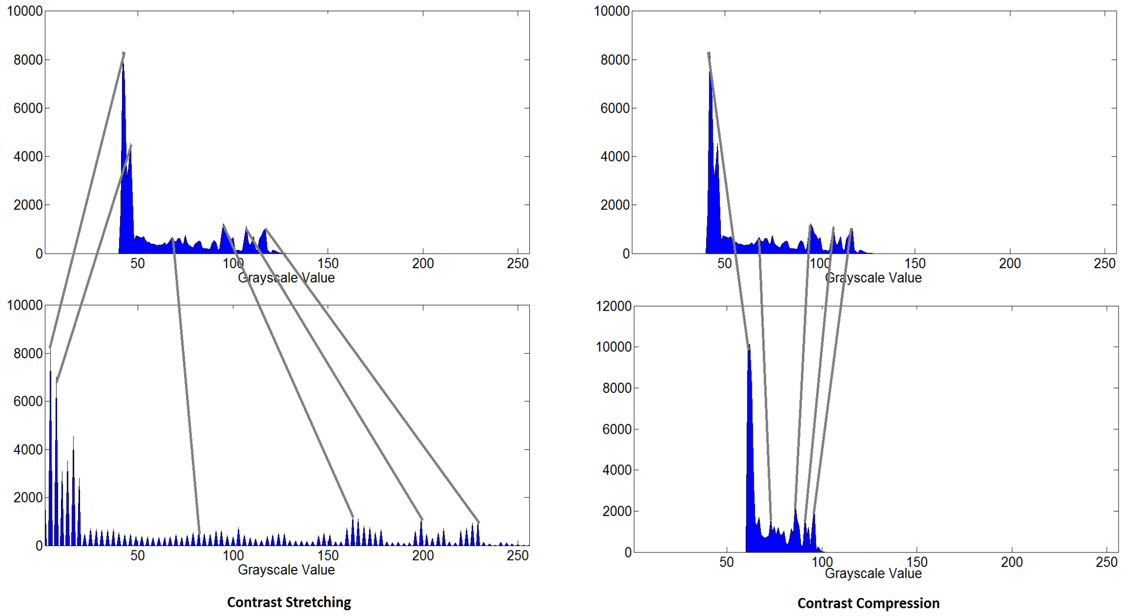

(a)

Figure 4.2 Representation of contrast stretching/ compressing (windowing)

$$L_{s1} = W_{center} - \frac{W_{center}}{2} \tag{4.1}$$

$$L_{sm} = W_{center} + \frac{W_{center}}{2} \tag{4.2}$$

The mathematical equation representing windowing can be written as,

$$L_d = \left(L_s - W_{center} - \frac{W_{center}}{2} \right) \times \left(\frac{255 - 0}{W_{width}} \right) \tag{4.3}$$

Where, L_d and L_s represent the source and destination grayscale values respectively. Windowing also performs contrast stretching/ compression based on the values of m and n. Contrast stretching occurs when the range of grayscale values (m) selected to be displayed is smaller than that of the display monitor (n) and vice versa (Figure. 4.2). The shorter the span of grayscale values to be mapped, the higher the contrast enhancement achieved. The enhancement between the various tissue types helps the radiologists to identify subtle discrepancies in the tissues which were earlier very difficult to detect.

The radiologists use the windowed CT scans to detect any signs of early infarct. The most important sign of infarction is the loss of gray/ white matter interface which can be really difficult to spot when windowed at the entire soft tissue range (std. settings) but when viewed under appropriate (reduced) window settings, become relatively easier to detect. The shortening of the window width decreases the amount of tissues lying in the window range. Therefore, in order to look for the tissue discrepancies across the entire tissue range, the doctors must manually slide the window to cover the entire intensity

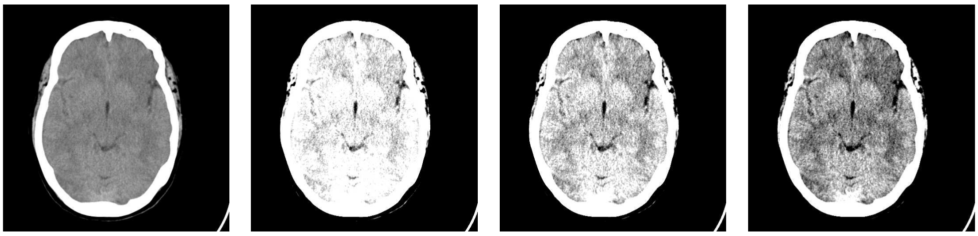

(a) Stroke standard window (b) (Window Center - 1050, Width - 25) (c) (1055, 25) (d) (1060, 25)

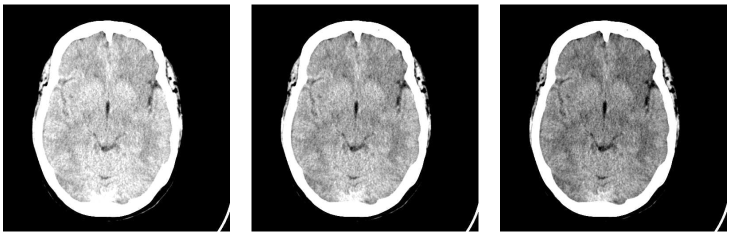

(e) (1050, 40) (f) (1055, 40) (g) (1060, 40)

Figure 4.3 Stroke appearance under reduced window settings (center, width).

range. The selection of appropriate window width and center resembles a trial and error process whose accuracy depends on the experience of the radiologists [50]. The main reason for experience playing such a large role in window selection is that windowing, while achieving contrast enhancement also tends to increase the noise and artifacts in the scan. All these factors compounded by the poor tissue contrast offered by the CT may adversely affect the judgment of doctors. With increased experience and training, the doctors learn to distinguish between the true ischemic signs and the artifacts. Figure. 4.3 shows the appearance of an early infarct scan under different window settings. Moreover, Krupinski et al. [18] mentions the effect of workload and fatigue on the detection accuracy of the radiologists which may result in missed infarct cases. Although the study presents the case of fracture detection, a similar observation may also be derived for hyperacute infarct where the affected tissue mimic the property of normal tissues and require higher concentration levels to detect amid all the noise and artifacts. Automatic enhancement of affected tissue will therefore go a long way in minimizing all these risks.

As discussed in chapter. 2, a lot of research has gone into finding an appropriate contrast enhancement. Although non-linear enhancements increase the contrast between the normal and abnormal tissue appreciably, they also tend to introduce unwanted artifacts and noise [20]. These can adversely influence the decision making of the radiologists. One way of countering the errors can be through increasing familiarity with the concerned method but making it a standard like the current prevalent windowing process is too much of an ask. Therefore the best way to increase the detection rate of early infarct is through automating the tried and tested windowing process currently used by radiologists.

The purpose of this study was to develop an algorithm to improve the diagnostic accuracy of early infarct by maximizing perceptual contrast between normal and abnormal tissues using linear enhancement of tissue intensities. We aim at minimizing the 'experience' factor in the current detection process.

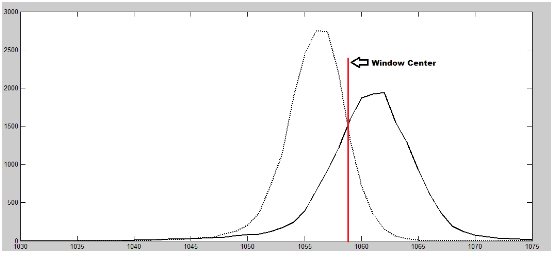

Figure 4.4 Histograms of V_i and V_{ic}

In the coming sections, we present two different strategies for determining the optimal window settings based on 1. Region-level and 2. Pixel-level properties of the brain CT. Both the tracks leverage the asymmetrical subtle changes that occur during the early times by emphasizing them and thus help distinguish between normal and abnormal (stroke affected) tissue. These strategies although being stroke specific, can also be applied to accentuate the differences in similar other abnormalities of the tissues.

4.2 Region Based Windowing

The region based method takes off from where the hyperacute detection method stopped in chapter. 3. At the end of the detection process, we are left with stroke affected tissues. The required window settings are then determined as follows. Given a detected infarct volume V_i, its counterpart volume V_{ic} is first extracted from the other hemisphere. Assuming this represents a normal volume, maximum perceptual contrast between the normal and affected tissue regions is achieved by setting the window center at a point such that the distribution is balanced about this center. This is achieved by computing intensity histograms of V_i and V_{ic} and finding the bin corresponding to the point of maximum overlap between the histograms (Figure. 4.4). The window width can be chosen according to the tissue information desired by the radiologist as the above window center will provide maximum contrast irrespective of width. Figure. 4.5 shows the test images under modified window settings (window width is taken as 25 H.U.). In the next section, we present a different approach to windowing using the pixel level properties.

4.3 Pixel Based Windowing

Pixel-based windowing is a novel approach inspired by ideas of binary image thresholding. In thresholding, the aim is to divide the image pixels into two exclusive classes of intensities based on optimization of a criterion function. In our method, we achieve best possible windowing for aiding stroke detection by selecting an intensity range which maximizes the difference in distribution of pixels in left and right hemispheres. Although the underlying principles are the same, the proposed method differs from thresholding as it chooses a single class of intensities based on two images whereas thresholding

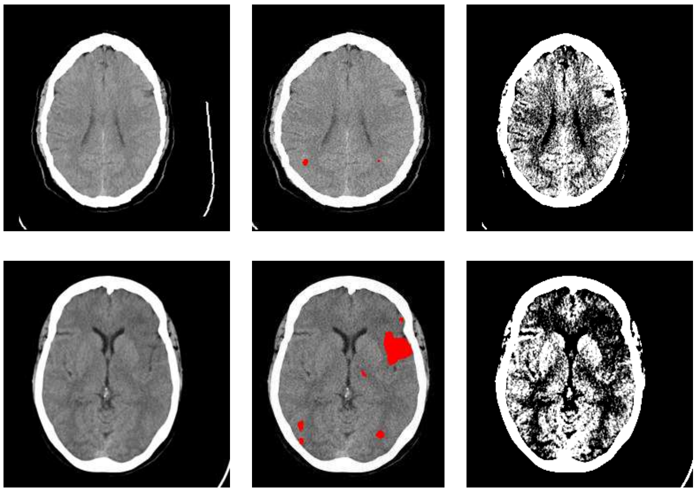

Figure 4.5 Results of proposed algorithm on normal (row: 1) and hyperacute (row: 2).The columns 1-3 depict input image, detected abnormality (overlapped on input image) and the original image under modified viewing window settings respectively.

chooses two classes of intensities based on a single image. The window settings (center and level) are then computed from the obtained intensity range.

Since the early days, a variety of approaches have been proposed for thresholding a gray scale image. Some of the most widely used among them are Otsu, Minimum error thresholding, Entropy based methods etc. All these methods have different strengths and weakness. A more detailed explanation can be found in [37]. We base our windowing technique on a recently proposed thresholding approach based on parzen-window estimate [46]. The main reason for selecting the above was the ease with which the framework could be exploited to perform thresholding on a pair of images rather than on a single image. Other factors which weighed favorably towards its selection were the incorporation of spatial information of pixels apart from the better thresholding results compared to other commonly used approaches. Incorporation of spatial information was necessary for detecting the disturbances in the contra-lateral symmetry. In the coming sections, we first describe the theory behind parzen window estimation and how it's used in context of images.

4.3.0.1 Parzen Window

The parzen window based non-parametric density estimation approach was first proposed by [35], [29]. We first describe the parzen window concept when applied to images. Let I be an image of size m x n having gray values from 1 to L. We define a pixel location as $\{$(x,y) : x ϵ (1,2,...,m), y ϵ (1,2,...,n)$\}$ and its value as f(x,y) ϵ (1,2,3,...,L). Let ω_i = $\{$(x,y) : f(x,y)=i$\}$ and $C_i = |\omega_i|$ giving N, total number of pixels as N = $\sum_{i=1}^{L} C_i$. The probability density function $P(x, y)$ at (x,y) can be estimated using parzen window as

$$\text{P(x,y)}= \sum_{i=1}^{L} P(x,y,\omega_i) = \sum_{i=1}^{L} P(\omega_i)P(x,y|\omega_i) \tag{4.4}$$

Where,

$$P(x,y|\omega_i) = \frac{1}{C_i}\sum_{j=1}^{C_i}\frac{1}{V_{C_i}}K\left(x,y;x_j,y_j;h_{C_i}^d\right) \tag{4.5}$$

$$P(\omega_i) = \frac{C_i}{N} \tag{4.6}$$

Where K (.) is called a kernel function, V_{C_i} denotes the volume of d-dimension hypercube having edge h_{Ci}. Since we are dealing with 2 dimensions here, d is taken as 2 and V_{Ci} = h_{Ci}^2 [9]. The kernel function must be designed in a way that is inversely proportion to distance between (x, y) and (x_j, y_j) so that farther pixels contribute less towards the density estimate and vice versa. In our approach we take the kernel function to be a Gaussian. Most of the parzen density based approaches suggest V_{C_i} = $1/\sqrt{C_i}$ as a good estimate. Next, we will describe how the parzen window principle in incorporated in our windowing approach.

$$K\left(x,y;x_j,y_j;h_{C_i}^2\right) = \frac{1}{\sqrt{2\pi}}\exp\left(-\frac{(x-x_j)^2+(y-y_j)^2}{2h_{C_i}^2}\right) \tag{4.7}$$

4.3.0.2 Parzen Based Windowing

As mentioned earlier, one of the earliest visible signs of acute infarct on CT includes the disturbance in the contralaterally similar distribution of white and gray matter. The idea is to exploit this phenomenon to find the intensity range where this disturbance is most perceptible. Let W_c and W_w be the target window center and width respectively. The present windowing procedure used by radiologists takes the tissues which lie in the intensity range $\omega_{w,c}$ = [W_c - W_w/2, W_c+W_w/2] and c, w $\epsilon[1, L]$ and then stretches the intensity range to the visible intensity range (0-255). Our approach aims at finding the optimal intensity range ω_t based on a criterion function which maximizes the disturbance in left and right hemisphere images. Let P_l and P_r denote the probability density function of pixels in left and right hemispheres respectively, in the intensity range $\omega_{w,c}$ and can be estimated using parzen window as

$$P_l = \sum_{k\epsilon\omega_{left}} P_l\left(x_k,y_k\right) = \sum_{k\epsilon\omega_{left}}\frac{1}{N}\sum_{i\epsilon\omega_{w,c}}\sum_{j=1}^{C_{il}}\frac{1}{V_{C_{il}}}K\left(x_k,y_k;x_j,y_j;h_{C_{il}}^2\right) \tag{4.8}$$

$$P_r = \sum_{k\epsilon\omega_{right}} P_r\left(x_k,y_k\right) = \sum_{k\epsilon\omega_{right}}\frac{1}{N}\sum_{i\epsilon\omega_{w,c}}\sum_{j=1}^{C_{ir}}\frac{1}{V_{C_{ir}}}K\left(x_k,y_k;x_j,y_j;h_{C_{ir}}^2\right) \tag{4.9}$$

Where, ω_{left} and ω_{right} are the set of pixels in left and right hemispherical image. Now we need to determine a criterion function whose optimization will lead us to the optimal window settings. The simplest mathematical function that ensures maximum difference in the probability distributions of left and right hemispheres is $|(P_l - P_r)|$.

$$(width, center)_{optimum} = argmax_{w,c}|(P_l - P_r)| \tag{4.10}$$

The above criterion function is bi-variable in w, c and further increases the computational complexity of the already computationally intensive parzen estimate. The criterion function, however, can be reduced to a single variable form in the special case of brain by utilizing some domain knowledge. Ever since the advent of soft copy of CT, much work has gone into finding the best possible predetermined window parameters. These parameters, especially window width, ensure that noise and other artifacts that get accentuated with the windowing process do not adversely affect the radiologist's judgment. In order to make sure our algorithm is immune to such damage, we limit the width parameter to the one designated by the stroke protocol (10) and then use the criterion function to find best possible window center. The complete algorithm is given below.

1. Threshold the given CT scan to obtain only the brain tissues and correct for rotation by finding the mid-sagittal plane (Section. 3.2).
2. Divide the given image into left and right hemispheres using the mid-sagittal plane.
3. Next for each gray level in the image as window center, i, compute t(i) = $|(P_l - P_r)|$ with the intensity range as [i-10,i+10].
4. Choose the gray level, i*, such that $t(i*) \leq t(i)$ for all $i \neq i*$.
5. Output the image with (i*,10) as window parameters (Figure. 4.6).

4.4 Results

4.4.1 Experiment Details

The windowing results obtained from Region-based (W_r) and Pixel-based (W_p) methods were compared by means of perception study conducted in an clinical environment. The results from the two automated methods were compared with each other as well as with the standard window settings (W_s, width 80 H.U. and center 40 H.U.). A set of 15 slices was selected from each of the hyperacute and normal dataset and each slice was presented randomly under the different window settings W_r, W_p and W_s to the radiologists. Since the region-based method performs enhancement only in cases in which it detects an infarct, all such slices from the above set (normal cases and missed infarct slices) were shown to the users with the window settings as: W_s. The inclusion of infarct cases which were missed by the region-based method gives us an opportunity to test the main advantage of pixel-based method over the

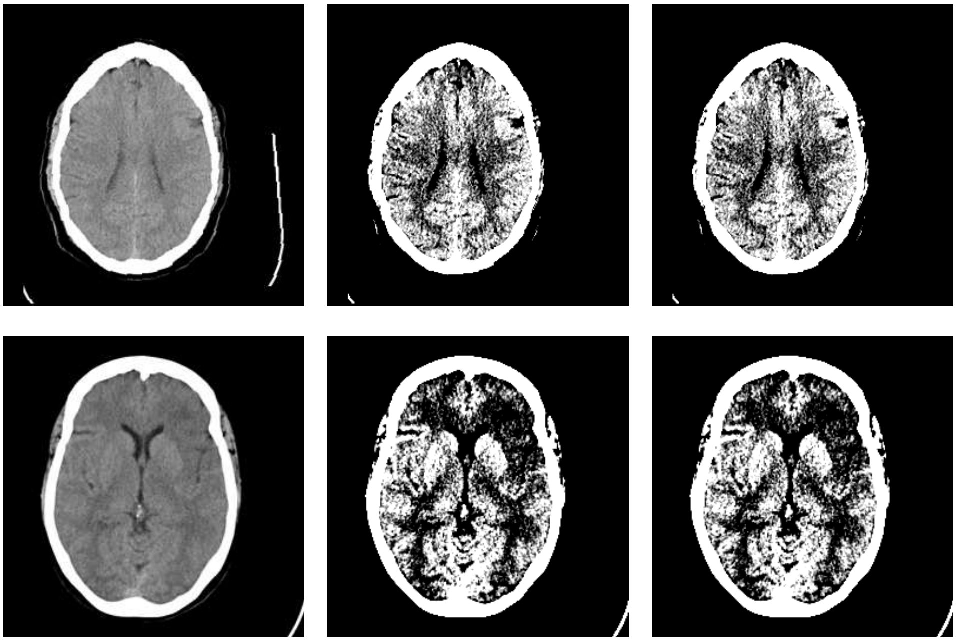

Figure 4.6 Results of proposed parzen-based windowing algorithm on normal (row: 1) and hyperacute (row: 2).The columns 1-3 depict input image, original image under modified viewing window settings obtained using parzen-based method and using region-level method respectively.

Reader	1			2			3			4		
Setting	W_p	W_r	W_s	W_p	W_r	W_s	W_p	W_r	W_s	W_p	W_r	W_s
Sensitivity	100	93.3	73.3	93.3	80	66.6	73.3	73.3	53.3	73.3	73.3	46.6
Specificity	100	100	93.3	100	100	86.6	100	100	80	93.3	93.3	73.3
Accuracy	100	96.6	83.33	96.6	90	76.6	86.6	86.6	66.6	83.3	83.3	60

Table 4.1 Clinical study results

region based method. In the current set of 15 abnormal slices, 2 of these slices were the ones having infarct region missed by the region-based method. Each slice was rated by 4 radiologists, having varied experience, in a blinded review for the presence of hyperacute infarct. Their response as well the time taken for decision was recorded. In compliance with similar clinical studies, the statistical significance of the results of the above experiment was also evaluated using two tailed student's t-test.

4.4.2 Discussion

Table. 4.1 shows the results of the clinical study. The results showcases the superior performance of both automated windowing methods (W_p, W_r) against the standard window setting. Average sensitivity showed statistically significant increase in the performance from 59.95% in case of W_s to 79.97%

and 84.97% in case of W_r and W_p respectively. (P = 0.034 for W_p, P = 0.040 for W_r, two-tailed students' t test.) The average specificity numbers also showed a rise from 83.3% (W_s) to 98.34% (W_r) and 98.34% (W_p). As seen with sensitivity, the specificity numbers also showed statistical significance in accordance with the students' test (p = 0.032 for W_r and W_p). The overall accuracy of the radiologists (measured in terms of the percentage of slices correctly identified) which was only around 71% under W_s increased to 91.6% (W_p, p = 0.024) and 89.16% (W_r, p = 0.034) in case of the automated methods. The above results showcase the increase in the performance of radiologists when viewing the test scans under automatically determined window settings. Moreover, the higher sensitivity numbers prove our earlier thoughts that the enhancement of test images are not achieved at the cost of specificity which certainly seem to the happen in case of non-linear enhancement. Also, there was no case where a correct identification of infarct under W_s was reversed when observed under W_p/W_r. The slight advantage in performance of pixel-based method is because of the presence of 2 stroke slices on which the region-based enhancement fails to perform the appropriate enhancement. These slices were having very small infarct which gets enhanced by the pixel-level method and thus gets detected by the experienced radiologists. Another thing to note is that the region based method provides same window parameters for the entire scan where as the pixel-level algorithm provides window parameters adapted to the disturbance in that particular slice. This way the pixel-level approach provides better enhancement of infarct tissues present in the border slices where the tissues are generally less hypodense than in the core infarct region.

The similarity in performance observed by both pixel and region-based methods is because both the methods aim for exploiting essentially the same sign that points at the presence of infarct (blurring of gray/ white matter junction). In W_r, the algorithm first divides the brain tissues into gray/ white matter regions before comparing the overlap whereas, in W_p, the gray/ white matter are compared directly. The difference being, W_r requires a threshold to separate normally observed asymmetry from the asymmetry due to presence of stroke and hence in order to keep the false positives down, the algorithm misses cases in which the gray/ white matter asymmetry caused due to stroke is very weak. Hence the algorithm does not enhance these cases as they are classified as normal whereas the pixel-based method requires no such threshold and always produce enhancement no matter how weak the stroke is. Although since the pixel-level is local in nature, it does tend to get easily effected by the other small disturbances which are also present in the normal brain e.g. slight aberration in CSF distribution. As a result, though both the methods exploit the same early infarct signs, the enhancement achieved is slightly different mainly because of the difference in the position of the window center. The window centers obtained by the region-level method are generally more specific i.e. are more characteristic to the infarct region and also are generally on the left side of those obtained by the pixel-level approach on the Hounsfield number line. One probable disadvantage, from the algorithmic point of view is that both the windowing methods are computationally very expensive.

Chapter 5

Conclusions

In this thesis we presented a unified framework for automatic detection and classification of stroke from brain CT scans for both diagnostic and academic purposes. We also proposed two different image adaptive approaches for automatic enhancement of stroke affected tissues. In this chapter we will review the approaches and also present future directions in which the approaches can be improved.

5.1 Automatic Detection

We presented a unified hierarchical approach for automatic detection and classification of all types of stroke. Previously proposed approaches mostly relied on the characteristics of stroke affected tissues and thus cannot be applied across all types of stroke owing to large variation observed in the behavior of affected tissues relative to the normal ones. We therefore exploit a common property exhibited by both ischemic and hemorrhagic stroke. Our approach models the stroke as a disturbance in the otherwise similar distribution of brain tissue with respect to the mid-sagittal plane (MSP). We designed an easy to difficult perceptible method which identifies the most easily perceptible stroke at each hierarchical level resulting in the identification of first hemorrhage, chronic, acute and finally the least perceptible hyper-acute infarct. In order to correctly estimate the contra-lateral symmetry of brain tissues, we proposed a new robust MSP detection algorithm based on the physical structure of the skull. The method benefits from the fact that the physical structure unlike soft tissue symmetry rarely change in the event of stroke and thus can be used for more robust detection of MSP even in stroke affected patients. The first phase of the algorithm aims at detection of hemorrhage and chronic infarct. The affected tissues in these appear hyper- and hypodense respectively as compared to normal brain tissues. Since the affected tissues at this level are easily perceptible, a subsampled histogram based approach was proposed for their detection. The histogram comparison gives a broad idea of symmetry which gets disturbed only by the presence of affected tissue and remains unaffected by the usually present asymmetry in the normal brain. Thus the method works well in cases where an appreciable amount of affected tissue is present. Although the amount of false negatives (missed stroke cases) can be decreased by setting a low threshold value for histogram comparison, this might give rise to an increased number of false positives mainly due to the irregularities in the CSF distribution across the MSP. In future, to detect the smaller stroke tissues, we can go for a grid-based histogram comparison rather than comparing the entire histogram at the same time. The approach can be designed in a broad to narrow scenario where the symmetry comparison is done at several spatial levels (cell ->block ->grid) and then a final consolidated symmetry measure is prepared. The symmetry comparison at lower spatial level will ensure that even smaller infarcts get picked up. The false positive in this case can be eliminated using anatomical information about the CSF.

The next phase of the algorithm involves the detection of acute infarct. The acute infarct is less perceptible than the hemorrhage and chronic stroke and thus cannot be detected by histogram detection. We therefore propose a novel approach which exploits the fact that acute affected tissues contain more water and thus perceptually appear more ‘settled’ owing to them being slightly less granular than the normal tissues. We quantify this degree of ‘settledness’ based on the wavelet energy of the contra-lateral hemispheres. The approach gives high detection success but suffers from the same problem of being too broader like the first phase of the algorithm.

The third and the most important phase (from diagnostic point of view) of the algorithm deals with the detection of hyperacute infarct. The affected tissues at this stage mimic the properties of the white matter and thus cannot be differentiated from the normal white matter tissues in the intensity plane. We therefore perform the symmetry comparison on the spatial characteristics of the tissues which gives us the regions exhibiting loss of gray/ white matter differentiation. In order to compare the spatial characteristics, we proposed a novel idea of rough tissue segmentation which gives the broader arrangement of gray/ white matter tissues. The spatial distribution of the gray/ white matter tissues are then compared and a loss of symmetry is attributed to hyperacute stroke. The symmetry comparison is designed in such a way that it negates the effect of the roughness in segmentation of gray/ white matter tissues. The algorithm provides an appreciable recall rate but also reports a large number of false positives. As seen with other two phases, the smaller or less perceptible infarcts may sometimes pass undetected through the algorithm. A similar grid based approach in this case will probably not work in this case since the degree of asymmetry exhibited by hyperacute stroke in the missed slices was almost similar to the one exhibited by normal brain and will further increase the false positives.

5.2 Enhancement of Affected Tissue

Next, we proposed a novel auto-windowing approach to overcome the limitations observed by the automatic detection approach. The non-standard window parameters were determined automatically to ensure the maximum possible contrast between the normal and affected tissues. The window parameters were derived using two different approaches. The first approach used region level properties to determine the window parameters based on the intensity characteristics of the detected stroke regions in the hyperacute detection step. The other approach exploits the pixel properties of the brain CT and finds the window parameters which maximize the disturbance in tissue (pixel) distribution in the left and right hemisphere. Both the methods showcased encouraging improvement in the detection accuracy of the radiologists. Moreover the jump in performance was more in case of inexperienced radiologists as compared to the experienced ones. The method presents a way to counteract the effects of experience and loss in concentration due to fatigue etc. by automatically finding the best possible window settings. One of the drawbacks of region level approach is its inability to find the optimal window parameters when the detection algorithm fails to detect the infarct. The pixel level approach leaves the decision making to the radiologists and finds the parameters in every case. Although this ensures the enhancement of even smaller infarcts, the method might get influenced by the noise/artifacts in the image unlike the region based method which tries to remove them based on decision making. In the future, the clinical study conducted in chapter 4 can be done on a much larger scale to test the relative strengths of each algorithm. Also to gauge the real performance of the automatic windowing, the experiments must be conducted with scans under radiologist-modified window settings rather than with standard window settings as is the case in chapter 4. Even though the windowing algorithm was developed keeping in mind its application for detection of early infarct on CT, it can be easily used in other pathology cases which present similar challenges. A very recent study conducted by [43] came to a conclusion that in spite of all the technological advances, stroke windows still continue to be a powerful tool in detection of a number of brain pathologies and must be a critical part of all head CT examination and not only limited to brain stroke. This encouraged us to look for similar problems in brain. One such problem that was looked at, was the early detection of brain tumor which looks similar to gray matter (hyperdense) in the early stages of its development (Figure. 5.1). Initial enhancement results obtained using our windowing approach are very encouraging and indicate a similar quality of enhancement being achieved in the case of tumors as with the hyperacute infarct. Although a more thorough evaluation will be required in order to gauge the performance in case of tumor analysis. Moreover, there is also a provision for extending the windowing process to other parts of human body which exhibit some or other kind of contra-lateral symmetry.

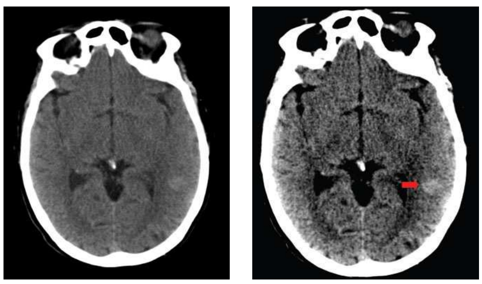

(a) Standard window settings (b) Non standard window settings

Figure 5.1 Appearance of early tumor lesions on CT scan [43]

Related Publications

- *”A method for automatic detection and classification of stroke from brain CT images”, M. Chawla, S. Sharma, J. Sivaswamy, Kishore L.T, International Conference of the IEEE Engineering in Medicine and Biology Society, 2009*
- *”Automatic Detection of Early Infarct from Brain CT”, S. Sharma, J. Sivaswamy, International Symposium on Medical Imaging in conjunction with ICVGIP 2010.*
- *”Assisting acute infarct detection from non-contrast CT using image adaptive window setting”, S. Sharma, J. Sivaswamy, R. Power, L. T. Kishore, Medical Image Perception Conference, 2011.*

Bibliography

[1] J. E. Barnes. Characteristics and control of contrast in CT. *Radiographics*, 12(4):825–837, 1992.

[2] M. Bendszus, H. Urbach, B. Meyer, R. Schulthei, and L. Solymosi. Improved CT diagnosis of acute middle cerebral artery territory infarcts with density-difference analysis. *Neuroradiology*, 39:127–131, 1997. 10.1007/s002340050379.

[3] M. Berthod, Z. Kato, S. Yu, and J. Zerubia. Bayesian image classification using markov random-fields. *Image and Vision Computing*, 14(4):285–295, May 1996.

[4] T. Chan. Computer aided detection of small acute intracranial hemorrhage on computer tomography of brain. *Computerized Medical Imaging and Graphics*, 4-5:285–298, July 2007.

[5] V. Choksi, D. J. Quint, P. Maly-Sundgren, and E. Hoeffner. Imaging of acute stroke. *Applied Radiology*, 34(2):10–19, 2005.

[6] D. Cosic and S. Loncaric. Computer system for quantitative analysis of ICH from CT head images. *In Proceedings of the 19th Annual Int'l Conference of the IEEE EMBS*, 1997.

[7] H. Demirel, C. Ozcinar, and G. Anbarjafari. Satellite image contrast enhancement using discrete wavelet transform and singular value decomposition. *IEEE GRS Letters*, 7(2):333 –337, April 2010.

[8] A. P. Dhawan, S. Loncaric, K. Hitt, J. Broderick, and T. Brott. Image analysis and 3-d visualization of intracerebral brain hemorrhage. *Proceedings of the Sixth Annual IEEE Symposium on Computer-Based Medical Systems*, pages 140–145, 1993.

[9] O. Duda, P. Hart, and D. Stork. *Pattern Classification*. USA: John Wiley and Sons, 2000.

[10] M. El-Melegy, Y. Hasan, and H. Mokhtar. MRI brain tissues segmentation using non-parametric technique. pages 185 –190. ICCES 2008, 25-27 2008.

[11] L. M. Fayad, Y. Jin, A. F. Laine, Y. M. Berkmen, G. D. Pearson, B. Freedman, and R. Van Heertum. Chest CT window settings with multiscale adaptive histogram equalization: Pilot study. *Radiology*, 223(3):845–852, 2002.

[12] J. Fiebach, P. Schellinger, O. Jansen, M. Meyer, P. Wilde, J. Bender, P. Schramm, E. Jttler, J. Oehler, M. Hartmann, S. Hhnel, M. Knauth, W. Hacke, and K. Sartor. CT and diffusion-weighted MR imaging in randomized order. *Stroke*, 33(9):2206–2210, 2002.

[13] M. Fisher and M. Ginsberg. Current concepts of the ischemic penumbra: Introduction. *Stroke*, 35:2657–2658, 2004.

[14] S. Geman and D. Geman. Stochastic relaxation, gibbs distributions, and the bayesian restoration of images. *PAMI*, PAMI-6(6):721 –741, nov. 1984.

[15] J. M. Gomori and I. Steiner. Non-linear CT windows. *Computerized Radiology*, 11(1):21 – 27, 1987.

[16] J. M. Hammersley and P. Clifford. Markov field on finite graphs and lattices. 1971.

[17] E. Hudyma and G. Terlikowski. Computer-aided detecting of early strokes and its evaluation on the base of CT images. pages 251–254. IMCSIT 2008, Oct. 2008.

[18] E. A. Krupinski, K. S. Berbaum, R. T. Caldwell, K. M. Schartz, and J. Kim. Long radiology workdays reduce detection and accommodation accuracy. *Journal of the American College of Radiology*, 7:698–704, 2010.

[19] Y. Lee, N. Takahashi, D.-Y. Tsai, and K. Ishii. Adaptive partial median filter for early CT signs of acute cerebral infarction. *IJCARS*, 2:2:105–115, June 2007.

[20] J. L. Lehr and P. Capek. Histogram equalization of CT images. *Radiology*, 154(1):163–169, 1985.

[21] M. H. Lev, J. Farkas, J. J. Gemmete, S. T. Hossain, G. J. Hunter, W. J. Koroshetz, and R. G. Gonzalez. Acute stroke: Improved nonenhanced CT detection: Benefits of soft-copy interpretation by using variable window width and center level settings. *Radiology*, 213(1):150–155, 1999.

[22] S. Z. Li. Modeling image analysis problems using markov random fields. volume 21 of *Handbook of Statistics*, chapter 13, pages 473 – 513. Elsevier, 2003.

[23] Y. Li, Q. Hu, J. Wu, and Z. Chen. A hybrid approach to detection of brain hemorrhage candidates from clinical head CT scans. *Sixth International Conference on Fuzzy Systems and Knowledge Discovery*, 2009.

[24] R. Liu, C. L. Tan, T. Y. Leong, C. K. Lee, B. C. Pang, C. Lim, Q. Tian, S. Tang, and Z. Zhang. Hemorrhage slices detection in brain CT images. *International Conference on Pattern Recognition*, pages 1–4, December 2008.

[25] Z. Majcenic and S. Loncaric. CT image labeling using simulated annealing algorithm. *IX European Signal Processing Conference, Island of Rhodos, Greece*, 1998.

[26] J. A. Maldjian, J. Chalela, S. E. Kasner, D. Liebeskind, and J. A. Detre. Automated CT segmentation and analysis for acute middle cerebral artery stroke. *AJNR, American Journal of Neuroradiology*, 22(6):1050–1055, 2001.

[27] M. Matesin, S. Loncaric, and D. Petravic. A rule-based approach to stoke lesion analysis from CT brain images. *Proceedings of the 2nd International Symposium on Image and Signal Processing and Analysis*, 2001.

[28] N. Otsu. A threshold selection method from gray-level histograms. *TSMC*, 9(1):62–66, jan. 1979.

[29] E. Parzen. On estimation of a probability density function and mode. *Annals Math. Statist.*, pages 1065–1076, 1962.

[30] Z. Peng, W. Wee, and J.-H. Lee. MR brain imaging segmentation based on spatial gaussian mixture model and markov random field. volume 1, pages I – 313–16. ICIP, 11-14 2005.

[31] N. Perez, J. Valdes, M. Guevara, and A. Silva. Spontaneous intracerebral hemorrhage image analysis methods: A survey. *Advances in Computational Vision and Medical Image Processing*, pages 235–251, 2009.

[32] J. M. Provenzale, R. Jahan, T. P. Naidich, and A. J. Fox. Assessment of the patient with hyperacute stroke: Imaging and therapy. *Radiology*, 229(2):347–359, 2003.

[33] A. Przelaskowski, K. Sklinda, P. Bargieł, J. Walecki, M. Biesiadko-Matuszewska, and M. Kazubek. Improved early stroke detection: Wavelet-based perception enhancement of computerized tomography exams. *Comput. Biol. Med.*, 37(4):524–533, 2007.

[34] A. Przelaskowski, J. Walecki, K. Szerewicz, and P. Bargiel. Acute stroke detection in unenhanced CT exams: perception enhancement by multi-scale approach. pages 94–95. Proceedings of National Conference on Physics and Engineering in the Present Medicine and Health Care, 2005.

[35] M. Rosenblatt. Remarks on some non parametric estimates of a density function. *Annals Math. Statist.*, pages 832–837, 1956.

[36] J. L. Saver. Time is brain–quantified. *Stroke*, 37(1):263–266, 2006.

[37] M. Sezgin and B. Sankur. Survey over image thresholding techniques and quantitative performance evaluation. *Journal of Electronic Imaging*, 13(1):146–168, 2004.

[38] H. Simon. Gray and white matter of the brain. [Online], June 2008.

[39] K. Sklinda, P. Bargiel, A. Przelaskowski, T. Bulski, J. Walecki, and P. Grieb. Multiscale extraction of hypodensity in hyperacute stroke. *Medical science monitor*, 13:1:5–10, May 2007.

[40] A. Srinivasan, M. Goyal, F. A. Azri, and C. Lum. State-of-the-art imaging of acute stroke. *Radiographics*, 26(suppl 1):S75–S95, October 2006.

[41] T. Tomsick, T. Brott, W. Barsan, J. Broderick, E. C. Haley, J. Spilker, and J. Khoury. Prognostic value of the hyperdense middle cerebral artery sign and stroke scale score before ultraearly thrombolytic therapy. *American Journal of Neuroradiology*, 17(1):79–85, 1996.

[42] T. A. Tomsick, T. G. Brott, A. A. Chambers, A. J. Fox, M. F. Gaskill, R. R. Lukin, C. W. Pleatman, J. G. Wiot, and E. Bourekas. Hyperdense middle cerebral artery sign on CT: efficacy in detecting middle cerebral artery thrombosis. *American Journal of Neuroradiology*, 11(3):473–7, 1990.

[43] P. J. Turner and G. Holdsworth. CT stroke window settings: an unfortunate misleading misnomer? *British Journal of Radiology*, 84(1008):1061–1066, 2011.

[44] A. Ušinskas, R. A. Dobrovolskis, and B. F. Tomandl. Ischemic stroke segmentation on CT images using joint features. *Informatica*, 15(2):283–290, 2004.

[45] S. Wall, M. Brant-Zawadzki, R. Jeffrey, and B. Barnes. High frequency CT findings within 24 hours after cerebral infarction. *American Journal of Roentgenology*, 138(2):307–311, 1982.

[46] S. Wang, F. lai Chung, and F. Xiong. A novel image thresholding method based on parzen window estimate. *Pattern Recognition*, 41(1):117 – 129, 2008.

[47] D. R. Weinberger, D. J. Luchins, J. Morihisa, and R. J. Wyatt. Asymmetrical volumes of the right and left frontal and occipital regions of the human brain. *Annals of Neurology*, 11:97–100, January 1982.

[48] Y. Xia, L. Wen, S. Eberl, M. Fulham, and D. Feng. Segmentation of dual modality brain PET/CT images using the MAP-MRF model. *IEEE 10th Workshop on Multimedia Signal Processing*, pages 107 –110, 2008.

[49] Y. Zhang, M. Brady, and S. Smith. Segmentation of brain MR images through a hidden markov random field model and the expectation-maximization algorithm. *TMI*, 20(1):45 –57, jan. 2001.

[50] R. D. Zimmerman. Stroke wars: Episode IV CT strikes back. *American Journal of Neuroradiology*, 25(8):1304–1309, 2004.